Flight Test of an L_1 Adaptive Controller on the NASA AirSTAR Flight Test Vehicle

Irene M. Gregory[1]
NASA Langley Research Center, Hampton, VA 23681-2199, USA

Enric Xargay[2]
University of Illinois at Urbana-Champaign, Urbana, Illinois 61801

Chengyu Cao[3]
University of Connecticut, Storrs, CT 06269

Naira Hovakimyan[4]
University of Illinois at Urbana-Champaign, Urbana, Illinois 61801

This paper presents results of a flight test of the L_1 adaptive control architecture designed to directly compensate for significant uncertain cross-coupling in nonlinear systems. The flight test was conducted on the subscale turbine powered Generic Transport Model that is an integral part of the Airborne Subscale Transport Aircraft Research system at the NASA Langley Research Center. The results presented are for piloted tasks performed during the flight test.

I. Introduction

One of the primary objectives of the Integrated Resilient Aircraft Control (IRAC) Project, under the auspices of the Aviation Safety Program, is to advance the state of the art in the adaptive control technology. Of particular interest is piloted flight under adverse conditions such as unusual attitudes, surface failures and structural damage. The IRAC Project is using subscale flight testing as an important tool in the evaluation of experimental adaptive control laws. This is particularly beneficial for the test and evaluation of control law performance beyond the edge of the normal flight envelope, where the risk of vehicle loss is high due to limited knowledge of nonlinear aerodynamics beyond stall and the potential for high structural loads. The Airborne Subscale Transport Aircraft Research (AirSTAR)[1-6] system at the NASA Langley Research Center has been designed to provide a flexible research environment with the ability to conduct rapid prototyping and testing for control algorithms in extremely adverse flight conditions. Moreover, to supplement this effort, high fidelity nonlinear aerodynamic models[7] for a subscale turbine powered Generic Transport Model (GTM) aircraft have been developed for an extended flight envelope depicted in Fig. 1. One essential objective for safe flight under adverse conditions is for the aircraft to never leave this extended flight envelope; once outside the boundary and in uncontrollable space, no guarantees for recovery can be made. Consequently, the adaptive controller should learn fast enough to keep the aircraft within the

[1] Senior Research Engineer, Dynamic Systems and Control Branch, AIAA Associate Fellow
[2] Graduate Student, Department of Aerospace Engineering, AIAA Student Member
[3] Assistant Professor, Department of Mechanical Engineering, AIAA Member
[4] Professor, Department of Mechanical Science and Engineering, AIAA Associate Fellow

extended flight envelope. This implies that the control law action in the initial 2-3 seconds after initiation of an adverse condition is the key to safe flight. The available models of the extended flight envelope and the ability to safely fly in this region make the GTM an excellent vehicle for an in-depth look at various aspects of adaptive control pertinent to piloted dynamically scaled turbine powered aircraft. This paper presents flight test results on the dynamically scaled turbofan powered GTM for the L_1 adaptive control architecture that directly compensates for significant cross-coupling in a multi-input and multi-output nonlinear system[8].

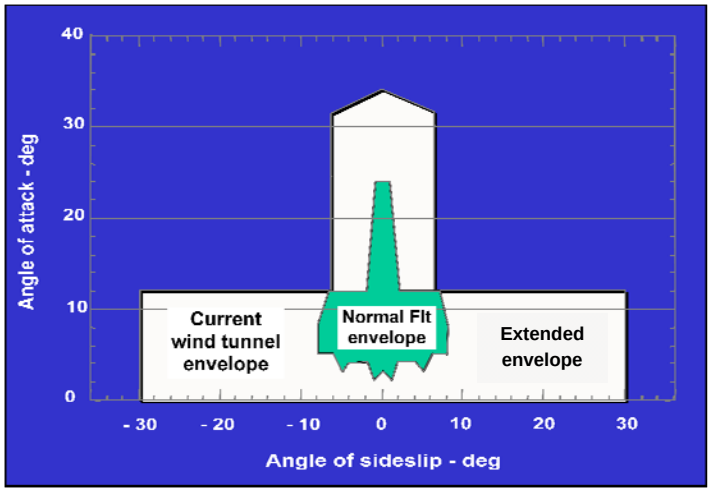

Figure 1. Extended flight envelope for the GTM based transport aircraft.

The L_1 adaptive control architecture was first proposed by Cao and Hovakimyan[9-14] and has been applied to a wide variety of flight vehicles over the last couple of years[15-18]. Unlike conventional adaptive controllers, the L_1 controller adapts fast, leading to desired transient and asymptotic tracking with guaranteed, bounded away from zero, positive time-delay stability margin. These features of the L_1 control theory make it an excellent candidate for validation and verification (V&V) in a realistic environment. Fast and robust adaptation in a robust way is a critical feature in creating appropriate control action within the first 2-3 seconds of adverse condition onset and keeping the aircraft from leaving the extended flight envelope.

The control objective for an L_1 adaptive controller is to achieve tracking for a variety of piloted tasks with guaranteed stability and robustness in the presence of uncertain dynamics, such as changes due to rapidly varying flight conditions during standard maneuvers, and unexpected failures. The control system presented here is a longitudinal axis angle of attack (AOA or α) command and lateral-directional axes roll rate (p) – sideslip angle (β) command augmentation system (CAS). Specific tasks that were flown and are presented in this paper include up and away flight and command tracking under various levels of aircraft stability degradation simultaneously in pitch and roll axes as well as angle of attack capture in post-stall high α flight regime. These flight tasks, changes to the aircraft dynamics and relevant flight conditions are described in detail in the paper.

The paper is organized as follows. Section II provides a brief AirSTAR flight test facility overview with emphasis on flight control law implementation environment. In Section III, the development of an L_1 all-adaptive control law, α, p-β CAS, is presented. Section IV describes the flight test results. Section V presents concluding remarks and describes future research plans.

II. AirSTAR Overview

AirSTAR is an integrated flight test infrastructure which utilizes remotely piloted, jet powered subscale models for flight testing. One particular use of AirSTAR is flight testing research control laws in adverse flight conditions. AirSTAR consists of a remotely piloted subscale test article, the Mobile Operations Station (MOS) (an integrated

ground station and control room), and a test range. Description of AirSTAR Concept of Operations can be found in Ref. 1-3. Basically, the research pilot executes a flight test plan from a research cockpit located in the MOS, which utilizes synthetic vision displays driven with aircraft sensor data. The research pilot uses a ground-based flight control system (FCS) that is connected to the aircraft through a telemetry link.

A. AirSTAR Infrastructure

Currently, AirSTAR's primary test aircraft is a 5.5% dynamically scaled twin-turbine powered generic transport model (GTM) shown in Fig 2. Dynamic scaling (i.e., similitude using equal Froude number and relative density between model-scale and full-scale) allows subscale flight test results to be applied to full-scale aircraft. This model (tail number T2) has a 6.5 ft wingspan, weighs 54 lbs at takeoff, and has a flight time of approximately 20 minutes. The aircraft is outfitted with full flight test instrumentation, including angle-of-attack and angle-of-sideslip vanes, sensors measuring static and dynamic pressure, control surface positions, rate gyros and accelerometers, a 6-DOF INS/GPS package, and engine instrumentation. Downlink data update rates vary from 5 Hz on the GPS data to 200 Hz on the data from analog sensors. Uplink commands are transmitted at 200 Hz.

Figure 2. AirSTAR Test Aircraft

The GTM aircraft has been extensively tested in the NASA Langley wind tunnels with particular emphasis on modeling nonlinear regions of the extended flight envelope well beyond nominal flight as well as developing a database for a number of structural damage scenarios[7,19]. The high fidelity nonlinear simulation of the GTM aircraft, built up from the extensive wind tunnel data, has been incorporated into the AirSTAR facility. Furthermore, that aircraft model has been updated with the data obtained during September 2009 flight test. With this capability AirSTAR provides a common research environment between flight and simulation with the only variable being whether the real GTM or its high fidelity simulation model is flying.

A. AirSTAR Flight Control System Structure

Of particular relevance to this paper is the flight control system development and implementation in the AirSTAR facility. The flight control system (FCS) is developed in The MathWorks MATLAB®/Simulink® environment and implemented on a ground-based dSPACE® real-time computer located in the MOS. Detailed description of the flight control system software development and implementation can be found in Refs. 2 and 3. A block diagram of the ground based flight software is provided for reference in Fig. 3. The commands from both pilots, safety pilot and research pilot, are input to the FCS, in addition to the aircraft sensor data, the output from the

Calculated Parameters subsystem, and the Caution & Warning subsystem. The Calculated Parameters subsystem calculates unmeasured quantities such as airspeed and altitude (from dynamic and static pressure) and applies center of gravity offset corrections to appropriate sensor data.

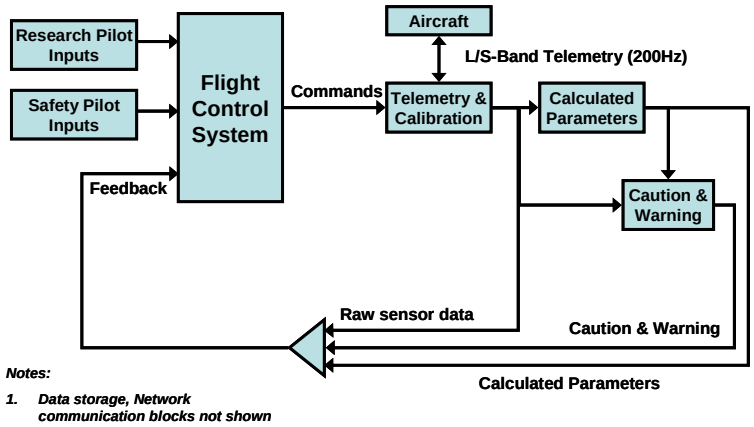

Figure 3. Block diagram of ground-based flight software.

It is important to note that the T2 aircraft has split surfaces - 4 elevator segments, inboard/outboard, left/right; right/left aileron; 2 rudder segments, upper/lower; flaps and spoilers. Segmented surfaces allow emulation of a range of failure that go beyond surface failures and include aerodynamic stability variations. The research flight control law (FCL) resides in the Flight Control System/Research Control Law Module, which is executed on a different processor and can contain any number of control laws, though only one can be operational at any one time. Furthermore, the current operational research flight envelope for the T2 Model, enforced by the loads protection system, is $600 \le Alt \le 1500$ ft and $40 \le V \le 100$ knots equivalent airspeed.

III. L_1 adaptive control laws for the GTM

The research control law developed for the GTM aircraft has, as its primary objective, achieving tracking for a variety of tasks with guaranteed stability and robustness in the presence of uncertain dynamics, such as changes due to rapidly varying flight conditions during standard maneuvers, and unexpected failures. Ideally, all of this must be achieved while providing Level I handling qualities under nominal as well as adverse flight conditions. An L_1 control system presented here is a three axes angle of attack (α), roll rate (p) – sideslip angle (β) command augmentation system. The α-command was chosen for reasons described below and the p-β command is one of the standard lateral-directional response types.

The simulation model is a full highly coupled nonlinear dynamic simulation, as previously mentioned. However, the desired control system behavior is to provide a decoupled response between longitudinal and lateral-directional axis, as well as, between lateral and directional axis as much as possible. The longitudinal α-command response type was chosen for two reasons. One, the operational baseline control law is α-command so the same response would make direct control law comparison relevant. And more importantly, other research tasks performed on the GTM require precise α control. However, α-command control law brings its own challenges to adaptive control formulation. In a typical aircraft, without direct lift devices, control acts through moment generating effectors, which implies that the uncertainty propagates through moment equations of motion and any uncertainty in α would generate significant cross-coupling effects. This cross-coupling uncertainty, also referred to as unmatched uncertainty, is uncertainty that does not enter through the range of the control effectiveness matrix B. In addition, the phugoid mode of a dynamically scaled aircraft is much closer in frequency to the short period dynamics than is the case for a full-scale aircraft. The combination of α-command response type and faster phugoid dynamics result in a

significant level of unmatched uncertainties. In fact, it is the desire for an α-command that motivated the development of an L_1 adaptive control architecture presented in this paper. Furthermore, for inner-loop FCS design, the effects of slow outer-loop variables (e.g. airspeed, pitch angle, bank angle) may appear as unmatched uncertainties in the dynamics of the fast inner-loop variables that are being regulated (e.g. angle of attack, sideslip angle, roll rate). Also, unmodeled nonlinearities, cross-coupling between channels, and dynamic asymmetries may introduce unmatched uncertainties in the inner-loop system dynamics. If the design of the inner-loop FCS does not account for these uncertainties, their effect on the inner-loop dynamics will require continuous compensation by the pilot, thereby increasing the pilot's workload. Therefore, automatic compensation for the undesirable effects of these unmatched uncertainties on the output of the system is critical to achieve desired performance, reduce pilot workload, and improve the aircraft's handling qualities.

Previous implementations of adaptive control in flight, whether JDAM missile[20-21] or RESTORE program[22-25], have been as a gain-scheduled augmentation to the existing gain-scheduled baseline controller. There are a number of excellent reasons for considering adaptive augmentation of gain-scheduled baseline controllers. However, since this design was a research control law for flight test, there is a great deal of interest in seeing what adaptation can do as a standalone control strategy, to stress the particular methodology and architecture to better understand the practical performance as well as the controller behavior at the limits. With a well designed robust baseline controller it is more difficult to assess how much adaptation is helping in providing stability and performance robustness and how much is the baseline controller contributing. Moreover, a baseline controller may hide potential deficiencies of the adaptive loop. In this sense, the open-loop characteristics of the GTM, which is a Level 1 FQ aircraft in its normal flight envelope, make this vehicle an excellent platform to test a standalone all-adaptive controller without any baseline in place. In fact, the development of adaptive controllers for stable systems entails fewer difficulties than the implementation of adaptive architectures for open-loop (highly) unstable platforms. In particular, the use of nonadaptive baseline controllers is critical for closed-loop performance improvement with satisfactory robustness margins when dealing with open-loop unstable aircraft subject to strict performance requirements. As an example of this discussion, Refs. 26 and 27 present the application of L_1 adaptive controllers as an augmentation loop for the existing baseline controllers on the X-48B and X-29 aircraft respectively.

Moreover, there is an interest in seeing how well the proposed L_1 architecture, which does not have any gain scheduling of the adaptation rate, can handle significant uncertainties due to cross-coupling in practice. Without a baseline present, all actions are those of an adaptive controller. Once this deeper insight is reached, adaptive augmentation, if desired, can be pursued with a much fuller understanding of the interactions and potential tradeoffs. Consequently the design presented here is a standalone L_1 all-adaptive controller introduced below.

A. Problem formulation [8,14]:

This section presents an overview of an L_1 adaptive control architecture used to design the flight control laws for the GTM aircraft. The detailed exposition of this architecture as well as all the relevant results can be found in Refs. 8 and 14.

Consider the following system dynamics:

$$
\begin{aligned}
&\dot{x}(t) = A_m x(t) + B_m\left(\mu(t) + f_1\left(x(t), z(t), t\right)\right) + B_{um} f_2\left(x(t), z(t), t\right), \quad x(0) = x_0 \\
&z(t) = g_0\left(x_z(t), t\right), \\
&\dot{x}_z(t) = g\left(x_z(t), x(t), t\right), \qquad x_z(0) = x_{z0} \\
&\mu(s) = G_a(s)u(s), \\
&y(t) = Cx(t),
\end{aligned}
\tag{1}
$$

where $x(t) \in \mathbb{R}^n$ is the system state vector (measured); $u(t) \in \mathbb{R}^m$ is the adaptive control signal ($m \le n$); $y(t) \in \mathbb{R}^m$ is the regulated output; A_m is a known Hurwitz $n \times n$ matrix that defines the desired dynamics for the closed-loop system; $B_m \in \mathbb{R}^{n \times m}$ is a known full-rank constant matrix, (A_m, B_m) controllable; $C \in \mathbb{R}^{mxn}$ is a known full-rank constant matrix, (A_m, C) is observable; $B_{um} \in \mathbb{R}^{n \times (n-m)}$ is a constant matrix such that $B_m^T B_{um} = 0$ and also $rank\left(\begin{bmatrix} B_m & B_{um} \end{bmatrix}\right) = n$; $z(t) \in \mathbb{R}^p$ and $x_z(t) \in \mathbb{R}^l$ are the output and the state vector of internal unmodeled dynamics; $G_a(s)$ is the uncertain system actuator dynamics; and $f_1 : \mathbb{R}^n \times \mathbb{R}^p \times \mathbb{R} \to \mathbb{R}^m$, $f_2 : \mathbb{R}^n \times \mathbb{R}^p \times \mathbb{R} \to \mathbb{R}^{(n-m)}$, $g_0 : \mathbb{R}^l \times \mathbb{R} \to \mathbb{R}^p$ and $g : \mathbb{R}^l \times \mathbb{R}^n \times \mathbb{R} \to \mathbb{R}^l$ are unknown nonlinear functions. The initial condition x_0 is assumed to be inside an arbitrary large known set, i.e. $\|x_0\| \le \rho_0 \le \infty$ for some $\rho_0 > 0$. In this problem formulation, $f_1(\cdot)$ represents the matched component of the uncertainties, whereas $B_{um} f_2(\cdot)$ represents the unmatched dynamics.

The control objective is to design an adaptive state feedback control law $u(t)$ to ensure that the system output response $y(t)$ tracks the output response $y_m(t)$ of the *desired system* defined as

$$M(s) \triangleq C(s\mathrm{I} - A_m)^{-1} B_m K_g(s),$$

where $K_g(s)$ is a feedforward prefilter, to a given bounded reference signal $r(t)$, *both in transient and steady-state*, while all other signals remain bounded. In particular, if the baseline feedforward prefilter $K_g(s)$ is chosen to be $K_g = -\left(CA_m^{-1}B_m\right)^{-1}$, the diagonal elements of the desired system transfer matrix $M(s)$ have DC gain equal to one, while off-diagonal elements have zero DC gain.

B. L_1 Adaptive Controller[8,14]

Similar to previous L_1 adaptive controllers, the philosophy of the L_1 adaptive state feedback controller for unmatched uncertainties is to obtain an estimate of the uncertainties and define a control signal which compensates for the effect of these uncertainties on the output $y(t)$ within the bandwidth of low-pass filters introduced in the feedback loop. These filters guarantee that the L_1 adaptive controller stays in the low-frequency range even in the presence of fast adaptation and large reference inputs. The choice of the low-pass filters leads to separation between performance and robustness. Adaptation is based on a piecewise constant adaptive law and uses the output of a state predictor to update the estimate of the uncertainties.

The elements of the L_1 adaptive control architecture are introduced below.

State predictor: We consider the following state predictor

$$\begin{aligned} \dot{\hat{x}}(t) &= A_m \hat{x}(t) + B_m\left(sat(\mu_0(t)) + \hat{\sigma}_m(t)\right) + B_{um}\hat{\sigma}_{um}(t) + K_{sp}\tilde{x}(t), \qquad \hat{x}(0) = x_0 \\ \mu_0(s) &= G_{a0}(s)u_{ad}(s) \\ \hat{y}(t) &= C\hat{x}(t) \end{aligned} \tag{2}$$

The state predictor replicates the closed-loop system structure, with the estimates $\hat{\sigma}_m(t) \in \mathbb{R}^m$ and $\hat{\sigma}_{um}(t) \in \mathbb{R}^{m-n}$ replacing the unknown parameters, $G_{a0}(s)$ is a known nominal actuator dynamics model, K_{sp} is such that $A_s \triangleq A_m + K_{sp}$ is a known Hurwitz matrix and $\tilde{x}(t) \triangleq \hat{x}(t) - x(t)$. The adaptive control signal $\mu_0(t)$ is amplitude limited and is calculated using the following static actuator model:

$$sat(\mu_0(t)) = \begin{cases} \mu_0(t), & |\mu_0(t)| \le u_{\max} \\ u_{\max} sign(\mu_0(t)), & |\mu_0(t)| > u_{\max} \end{cases}$$

Here $\mu_0(t)$ is the commanded control input and $u_{\max}$ defines amplitude saturation level.

Adaptive laws: The adaptive parameters are governed by the following piecewise constant adaptive law:

$$\hat{\sigma}_m(t) = \hat{\sigma}_m(kT_s), \quad \hat{\sigma}_{um}(t) = \hat{\sigma}_{um}(kT_s), \quad t \in [kT_s, (k+1)T_s]$$

$$\begin{bmatrix} \hat{\sigma}_m(kT_s) \\ \hat{\sigma}_{um}(kT_s) \end{bmatrix} = -\begin{bmatrix} B_m & B_{um} \end{bmatrix}^{-1} \Phi^{-1}(T_s) e^{A_m T_s} \tilde{x}(kT_s), \quad k = 0,1,2,\ldots \tag{3}$$

where T_s is the sampling rate of the model, $\Phi(T_s) = A_m^{-1}\left(e^{A_m T_s} - \mathrm{I}\right)$, and $\tilde{x}(t) = \hat{x}(t) - x(t)$ is updated every T_s sec.

Control law: The control law is generated as

$$\begin{aligned} u_{ad}(s) &= u_{ad\_m}(s) + u_{ad\_um}(s) + K_g(s) r(s) \\ &= -C_1(s)\hat{\sigma}_m(s) - C_2(s) H_m^{-1}(s) H_{um}(s) \hat{\sigma}_{um}(s) + K_g(s) r(s) \end{aligned} \tag{4}$$

where

$$H_m(s) \triangleq C\left(s\mathrm{I} - A_m\right)^{-1} B_m \qquad H_{um}(s) \triangleq C\left(s\mathrm{I} - A_m\right)^{-1} B_{um}$$

$C_1(s)$ is a strictly proper stable filter and $C_2(s)$ is selected to ensure that $C_2(s)H_m^{-1}(s)H_{um}(s)$ is also proper and stable. Furthermore, the transmission zeros of $H_m(s)$ need to lie in the open left-half plane. Regarding the structure of u_{ad_um} note that $H_{um}(s)\hat{\sigma}_{um}(s)$ is the estimated effect of the unmatched uncertainties on the output of the plant, while $-H_m^{-1}(s)H_{um}(s)\hat{\sigma}_{um}(s)$ would be the control signal needed to cancel this effect. The low-pass filters $C_1(s)$ and $C_2(s)$ serve to attenuate high frequencies in the adaptive control signals, and thus define the performance-stability robustness tradeoff. By designing a filter with a lower cutoff frequency, the robustness of the adaptive controller can be systematically tuned to increase the time-delay margin. Similarly a filter with a higher cutoff frequency will exhibit improved performance, at the cost of a reduced time-delay margin. The proof of the performance bounds of this architecture can be found in Ref. 8. This architecture has been applied to the GTM in a nonlinear simulation study of several cases of damaged aircraft.[28] A schematic representation is provided in Fig. 4.

C. Desired System Response for the GTM

The implementation of an L_1 all-adaptive control architecture is illustrated in Fig. 4. There is a longitudinal axis α-command control law and a lateral/directional axes p-β command control law. The desired system dynamics for the GTM are decoupled and are given by

$$\dot{x}_m = A_m x_m + B_m \delta_{cmd}$$

$$\begin{pmatrix} \dot{\alpha} \\ \dot{q} \end{pmatrix} = \begin{pmatrix} \frac{Z_\alpha}{V} & 1 + \frac{Z_q}{V} \\ M_\alpha & M_q \end{pmatrix} \begin{pmatrix} \alpha \\ q \end{pmatrix} + \begin{pmatrix} \frac{Z_{\delta_e}}{V} \\ M_{\delta_e} \end{pmatrix} \delta_e$$

in the longitudinal axis for α-command and

$$\begin{pmatrix}\dot{p}\\ \dot{\beta}\\ \dot{r}\end{pmatrix}=\begin{pmatrix}L_p & 0 & 0\\ 0 & Y_\beta/V & -1\\ 0 & N_\beta & N_r\end{pmatrix}\begin{pmatrix}p\\ \beta\\ r\end{pmatrix}+\begin{pmatrix}L_{\delta a} & L_{\delta r}\\ Y_{\delta a} & Y_{\delta r}\\ N_{\delta a} & N_{\delta r}\end{pmatrix}\begin{pmatrix}\delta_a\\ \delta_r\end{pmatrix}$$

for the lateral-directional axes p-β command. Matrices A_m and B_m are chosen such that A_m is Hurwitz and Level I handling qualities requirements[29] are satisfied. The design of the control laws incorporated the best practices from classical flight control law design by using command shaping filters and decoupling prefilters where appropriate. The low-pass filters are chosen as first order filter for $C_1(s)$ and two cascaded first order filters for $C_2(s)$; the bandwidth is adjusted based on the system dynamics and the desired performance vs. robustness tradeoff. Actuator dynamics are incorporated into the control laws as well.

An L_1 all-adaptive control law was designed for a nominal system at V=80 KEAS and Alt = 1000 ft. The nominal GTM model has 22 msec latency due to telemetry and sensor processing (6 msec on surface commands and 16 msec on sensor outputs). For design purposes the nominal system latency was increased 10% to 7msec and 18msec respectively. As indicated in Fig. 4 the telemetry uplink, commands, and downlink, sensors, are updated at 200Hz and the control law itself runs at 600Hz on a flight computer. One further item of note, an L_1 adaptive controller was designed strictly for pilot in the loop flying, hence the tuning was done for piloted flight and there is no outer loop compensation to hold altitude or pitch attitude. The results for a variety of test cases are presented in the next section.

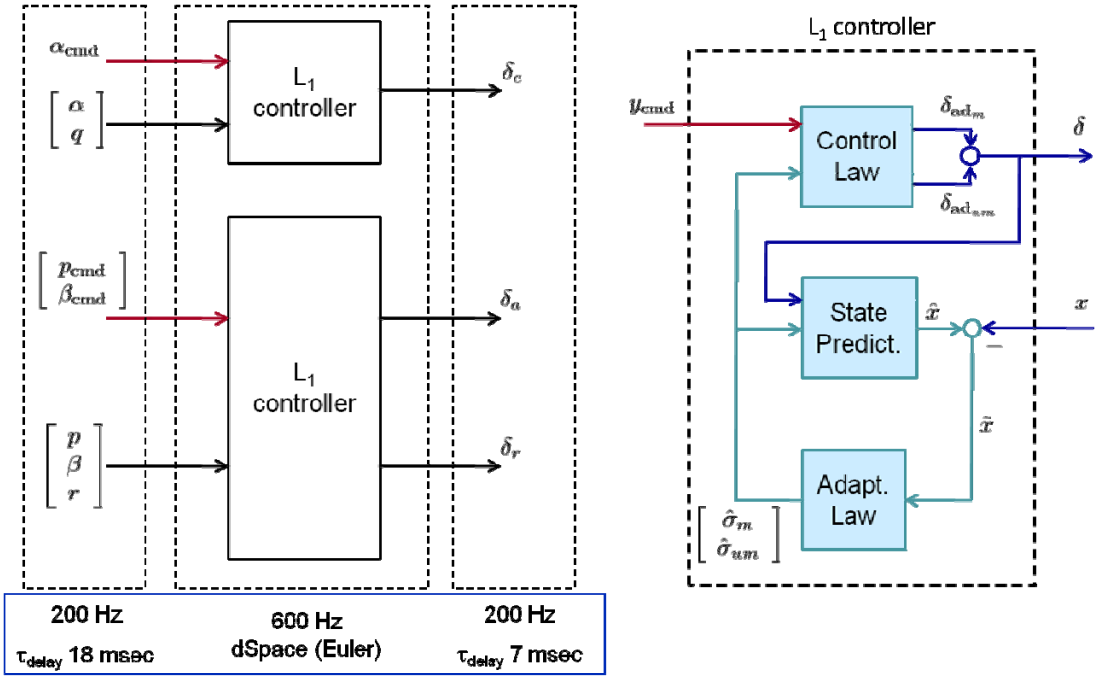

Figure 4. L_1 all-adaptive controller architecture.

IV. Flight test results

The material presented in this section are the results of a flight test of an L_1 all-adaptive controller flown on a twin turbine-powered, dynamically scaled GTM AirSTAR aircraft (tail number T2) conducted on 4 June 2010 at Ft. Pickett, VA. As mentioned previously the L_1 adaptive α, p-β command response control laws were designed for a nominal aircraft at a single flight condition (V=80 KEAS). The flight test was conducted in strict adherence to the

procedures outlined in the flight test plan[30] and the test cards[31], relevant sections of which are reproduced here to provide the necessary background to put the presented results in the appropriate context.

A. Flight Control Evaluation

Flight control law evaluation was conducted by evaluating command tracking performance in the presence of emulated faults. Commands were normal pilot inputs required to precisely fly a holding pattern and pitch and roll control stick doublet perturbations (superimposed on the pilot's stick commands). All the faults were emulated via software. The faults included command latency injection, degraded aircraft stability and control effectiveness. [30]

The degraded stability fault was a two axes degradation. Both longitudinal static stability and roll damping were simultaneously degraded. This was accomplished by simultaneously scheduling the inboard elevator segments as a function of angle of attack and the roll spoilers as a function of roll rate. Note that emulated loss-of-control effectiveness with these faults was implicit and the flight control law underwent a loss of pitch control effectiveness since all four elevator segments operate symmetrically for pitch control in the nominal aircraft. The stability degradation fault is not carried through the turns, so the fault is engaged on the straight legs followed by a wave train. The fault is then disengaged for the turn and the whole process is repeated on the next straight leg. The pitch axis wave train is an angle of attack command doublet through the stick (WT29) and the roll axis wave train is a roll rate doublet (WT30) tuned to produce roughly 30 degrees bank angle. The flight control law evaluation matrix is given in Table 1, where "1.3Vs1" is indicated airspeed value 30% above stall speed. [30] This speed depends on aircraft weight and is typically between 70 and 72 KIAS.

(1.3Vs1 + 5, 900 ft AGL) Racetrack or Figure 8 Patterns

	Task	1st straight leg	2nd straight leg	Turns
1	Latency Injection (5ms / 5 sec)	Fault Engaged Roll Doublet	Fault Engaged Pitch Doublet	Fault Engaged
2	$\Delta(C_{m\alpha}$ & $C_{lp}) \approx$ 00%	Fault Engaged Roll Doublet	Fault Engaged Pitch Doublet	Disengage Fault
3	$\Delta(C_{m\alpha}$ & $C_{lp}) \approx$ -50%	Fault Engaged Roll Doublet	Fault Engaged Pitch Doublet	Disengage Fault
4	$\Delta(C_{m\alpha}$ & $C_{lp}) \approx$ -75%	Fault Engaged Roll Doublet	Fault Engaged Pitch Doublet	Disengage Fault
5	$\Delta(C_{m\alpha}$ & $C_{lp}) \approx$ -100% (neutrally stable)	Fault Engaged Roll Doublet	Fault Engaged Pitch Doublet	Disengage Fault
6	$\Delta(C_{m\alpha}$ & $C_{lp}) \approx$ -125% (unstable)	Fault Engaged Roll Doublet	Fault Engaged Pitch Doublet	Disengage Fault

Table 1. Flight control law evaluation matrix

An L_1 all-adaptive control law flew in light turbulence during flight 23 of the GTM T2 aircraft. Fig. 5 shows flight 23 altitude and speed profiles from take off to landing with demarcation of portions flown by the safety pilot (SP) and the research pilot. An L_1 all-adaptive research control law was engaged in uninterrupted fashion for 12.5 minutes. Note the altitude excursions to 1200 feet and corresponding speed drops to 50 knots indicated airspeed which indicate high angle of attack flight described in the following section. One very important point of note, flight test results correlate well qualitatively with simulation, including the post-stall flight. This provides an extra degree of confidence to execute maneuvers at the edges of the flight envelope without an extensive and slow envelope expansion phase.

The following subsections describe tasks in the order they were flown and present flight data results. The presented data is raw sensor data without any filtering or other modifications. The aircraft instrumentation is highly

sensitive (especially the gyros) and the output is sampled at 200Hz, even though some of the sensor outputs are updated at only 50Hz. The data reflects this sensitivity in picking up even minor aircraft motion which is excited even by very light turbulence. One other item of note is an aggressive nature of the turns necessary to maximize available research time on straight legs and remain within the flight boundary. These 180 deg turns are characterized by 40-50 degrees of bank angle. The magnitude of roll rate commanded by the pilot to achieve the typical bank angle depends on the aircraft's proximity to the boundary and ranges from roughly 30 deg/sec to 80 deg/sec in couple of instances.

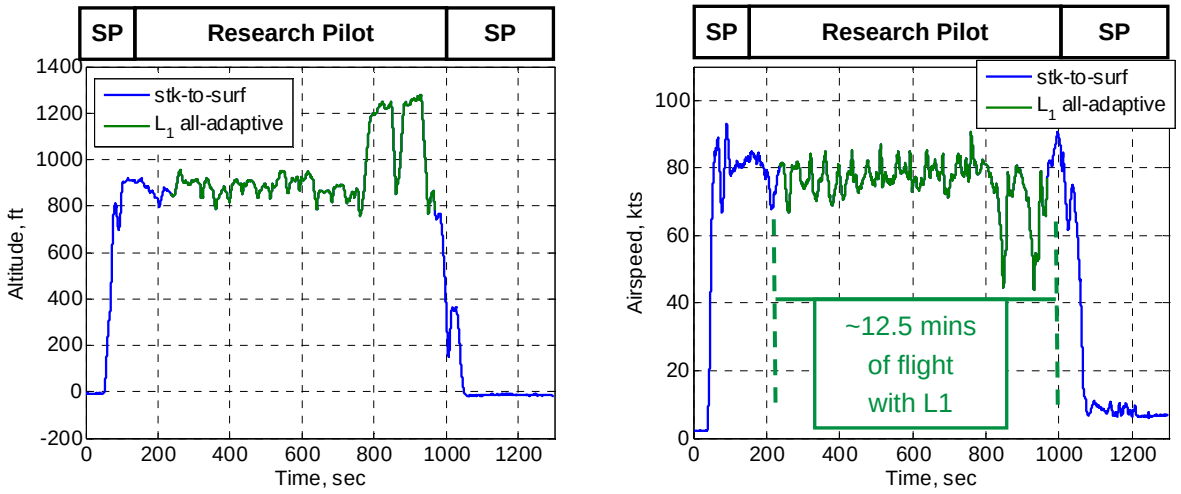

Figure 5. Flight 23 speed and altitude profiles showing an L_1 all-adaptive research flight control law.

1. Task 1 – Latency injection

The latency injection fault is used as one measure of robustness. All control design, irrespective of the methods used, must consider the tradeoff between performance and robustness. One of the defining features of adaptive control is its ability to recover performance in the presence of parametric uncertainty; hence, ability to handle parameter based stability degradation is considered a measure of performance. Thus, the classical control design tradeoff between robustness and performance is defined in this case as the tradeoff between tolerance of additional latency at the system input vs. ability to handle simultaneous Cmα/Clp stability degradation and 50% pitch axis control effectiveness reduction.

Once the safety pilot to research pilot handoff was complete and the research pilot flew half a race track pattern to familiarize himself with the research control law and established nominal testing condition, Vref+5 (77 KIAS) and 900 feet, the latency fault was engaged. Upon engagement there was an immediate additional 20 msec latency added at the plant input, i.e. the actuator commands were delayed. Every 5 seconds an additional 5 msec was added and the pattern continued until the aircraft response become unstable or close to it. Fig. 6 (a) and (b) provide pitch and roll axes response during the latency fault profile. Note that the latency fault was engaged around 286 seconds and the maneuver was abandoned at 394 seconds due to persistent roll rate oscillations of ± 20 deg/sec. Based on the recorded data an L_1 all-adaptive controller was robust to 0.125 seconds additional input latency and, furthermore, exhibited a graceful degradation in stability/performance as the latency was increased towards the limit. Moreover, the control system immediately returned to nominal performance as soon as the latency fault was abandoned. The latency fault engagement interval is delimited by cyan bracket in Fig. 6 (a) and (b). The plots in Fig. 6 (a) and (b) also illustrate the aircraft response during the turns, as the latency fault persisted, characterized by fairly aggressive roll rate commands to achieve a typical 40-50 degree bank and 8-10 degree angle of attack to maintain altitude. Wave trains in angle of attack command (WT 29) and roll rate command (WT30) were sequentially injected on the

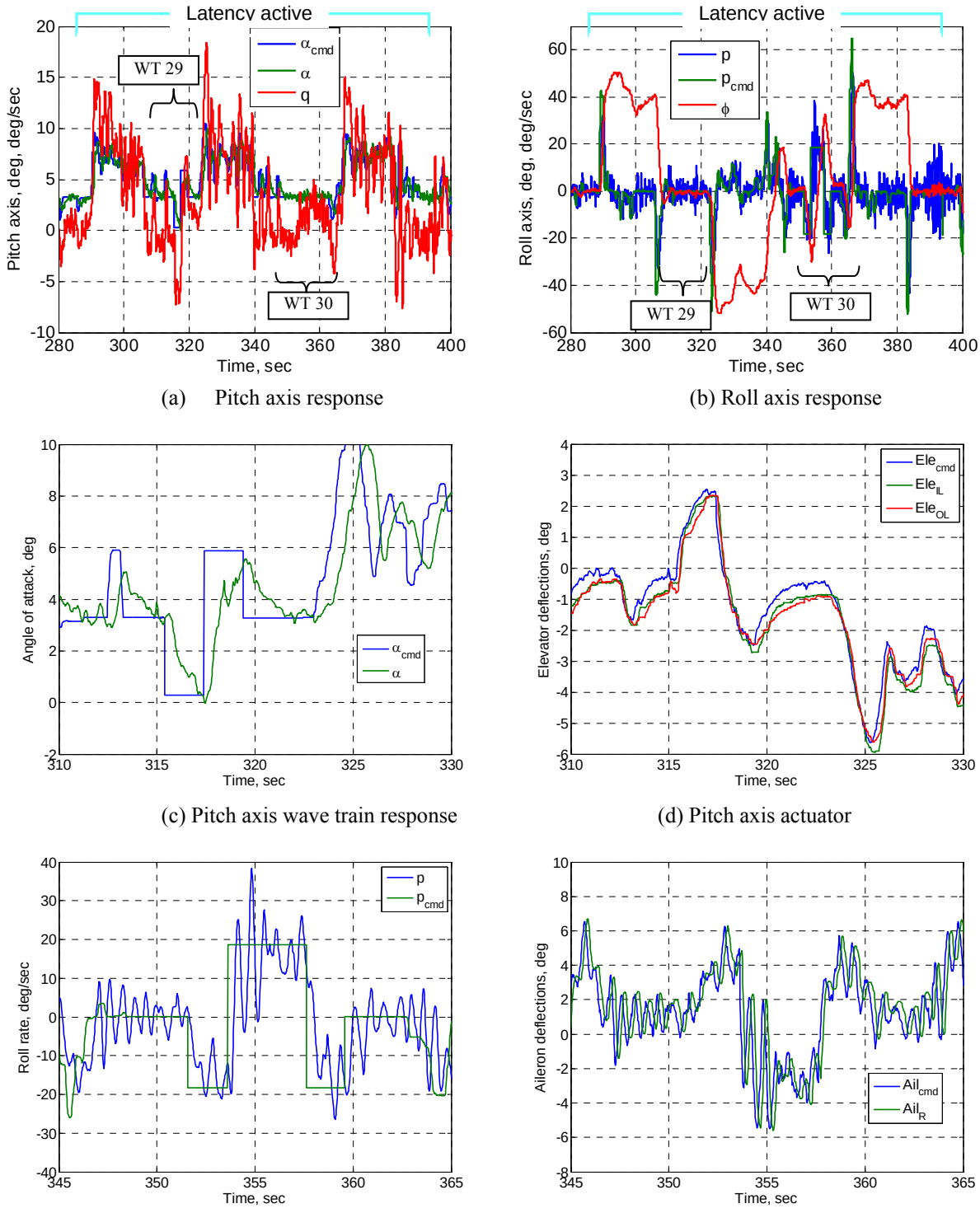

(a) Pitch axis response

(b) Roll axis response

(c) Pitch axis wave train response

(d) Pitch axis actuator

(e) Roll axis wave train response

(f) Roll axis actuator

Figure 6. Latency fault profile – maximum additional latency 0.125 seconds.

straight legs through the stick with the pilot flying hands off during the maneuver. Fig. 6 (c) and (e) illustrate the wave trains and the aircraft's response to these commands as the latency increased every 5 seconds. Actuator commands and measured actuator deflections for each axis, shown in Fig. 6 (d) and (f), exhibit a smooth (as much as

turbulence and mechanical linkages permit) lower frequency response. Note that Fig. 6 (d) shows both inboard and outboard left elevator response, the reason for both elevator segments will become apparent in stability degradation tasks.

2. Task - Nominal aircraft wave train injection

The next set of maneuvers performed was nominal aircraft response to wave trains in pitch and roll axis, angle of attack and roll rate commands respectively. The nominal flight in the race track pattern and the responses to the wave trains form the basis for comparison with aircraft under various degree of stability degradation. This task also presents an opportunity to illustrate typical aircraft response for a given research flight control law.

Fig. 7 shows 70 seconds of flight that includes both wave trains, one complete turn and part of another turn. The lack of pilot input during the wave train injection, manifested as a precise straight line doublet, can be observed in Fig. 7 (a) and (b). Moreover, note very small sideslip angle (β) maintained by an L_1 all-adaptive control law and the nonzero command that comes from vane calibration bias (Fig. 7 (c)). The surface commands during this flight segment are illustrated in Fig. 7 (d). One item of note, since the rudder is very powerful and can add significant load for small deflections, especially at higher speed, small amplitude for the rudder is highly desired.

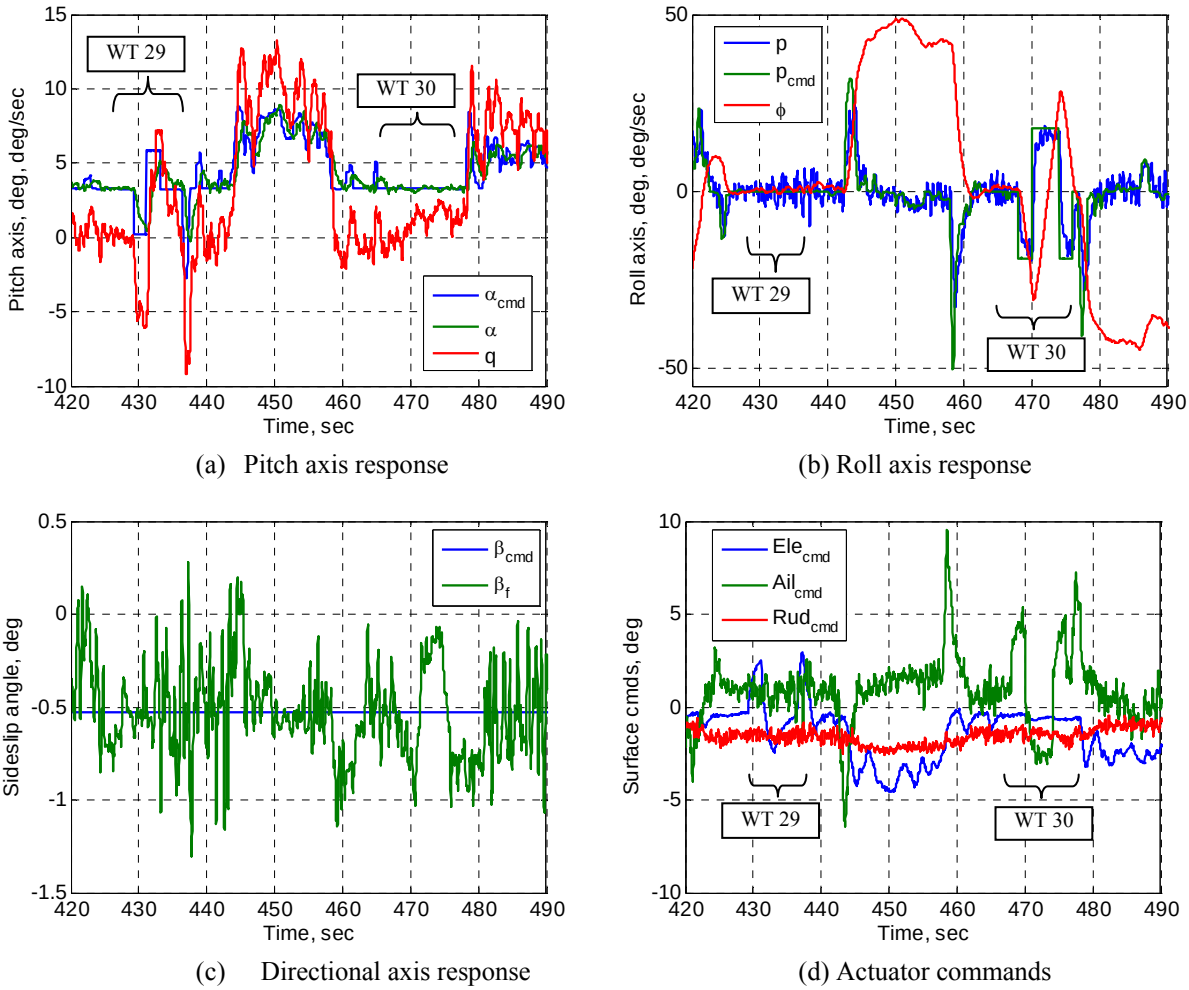

(a) Pitch axis response

(b) Roll axis response

(c) Directional axis response

(d) Actuator commands

Figure 7. Nominal aircraft wave train injection response

Another item of interest is how well the control law isolated the commanded response to the appropriate axis and minimized cross-coupling. The plots in Fig. 8 (a)-(d) show pitch axis wave train and corresponding lateral-directional response and in Fig. 8 (e)-(i) roll axis wave train and corresponding longitudinal-directional responses. Consider angle of attack wave train in Fig. 8 (a) and the smooth elevator command/response in Fig. 8 (c). The cross-coupling response in the lateral-directional axes is minimal with the roll and yaw rates never exceeding ±5 deg/sec which is considered within the turbulence/noise level, especially for the roll rate. The roll rate command doublet achieves 30 degrees bank angle as per design with a reasonable aileron command (Fig. 8 (e) and (g)). The pitch axis cross-coupling is minimal by design since the angle of attack is commanded to a constant value necessary to maintain nose up during the bank to bank maneuver. In the directional axis, sideslip angle is within 1 degree, $0 \le |\beta| \le 1$, and yaw rate is below ±10 deg/sec (Fig. 8 (f)). Hence, based on the responses in Fig. 8 (e)-(i) an L_1 all-adaptive control law generates minimal cross-coupling between the axes.

While looking at the angle of attack response to a commanded doublet (Fig. 8 (a)), it is important to consider the speed of the response in the context of a piloted aircraft. The original of tuning this control law was done in a batch simulation, with minimal attention to Mil-Standards, with the goal of tracking a doublet command as fast and as precise as possible. The initial comment from the pilot flying a control law thus tuned was "too sensitive in pitch." This comment has been consistent among a number of different pilots and different control laws tuned with the same goal in mind. After this initial evaluation, the control law was retuned with using Mil-Standards as a guide to achieve Level 1 flying qualities. During the control law development process, it was observed that even if the Mil-Standards for a fighter aircraft category were employed to tune the control law, it was still typically not sufficient to provide satisfactory pitch response. We speculate that the issue arises with the speed of GTM short period dynamics that are at least 3 times faster than those of an F-16 for example. The performance of the aircraft whose responses are shown in Figs. 7 and 8 has been judged to be Level 1. Pilot comment at the post flight 23 debrief was "a nice level 1 FQ airplane for light turbulence conditions." Consequently, angle of attack response to a commanded doublet is slow compared to what it is capable of.

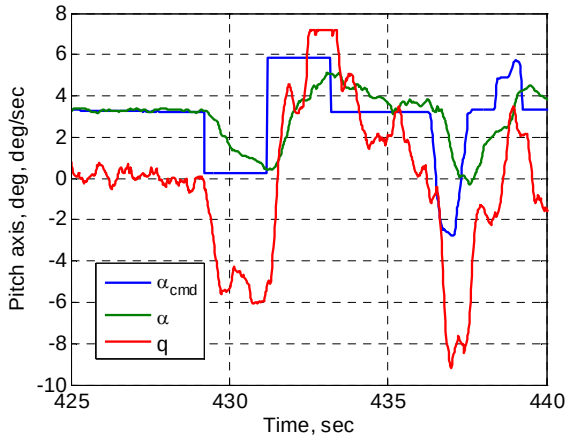

(a) Pitch axis wave train

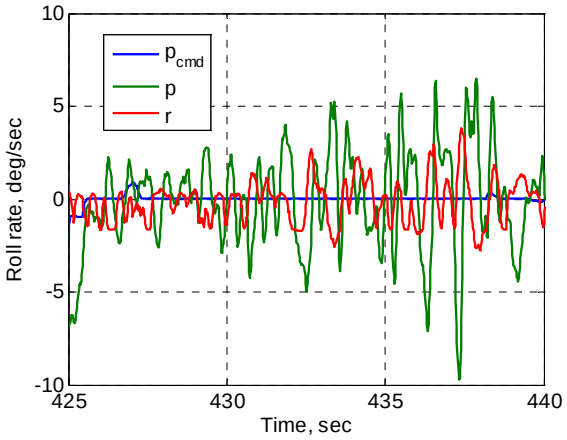

(b) Lateral-directional cross-coupling

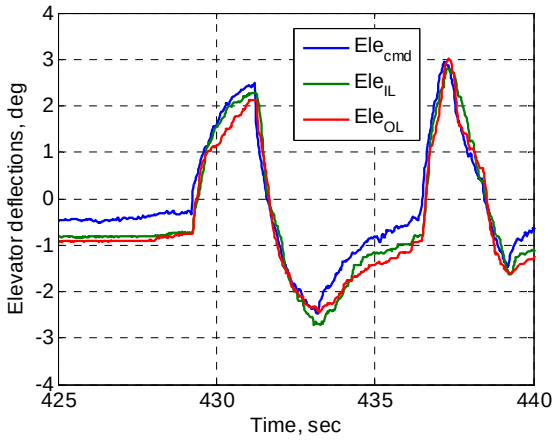

(c) Pitch axis actuators

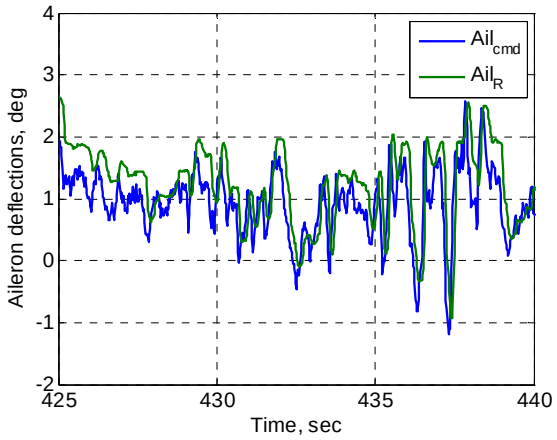

(d) Lateral-directional cross-coupling actuators

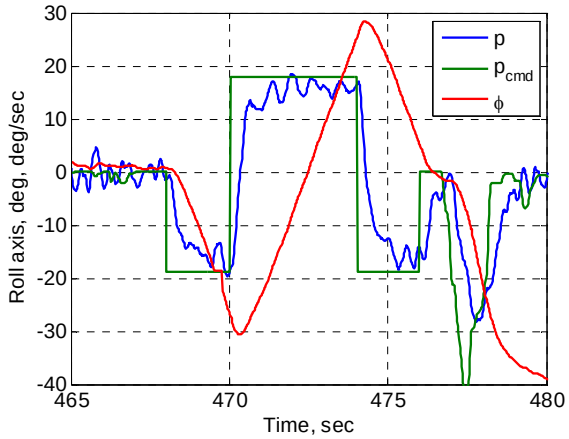

(e) Roll axis wave train

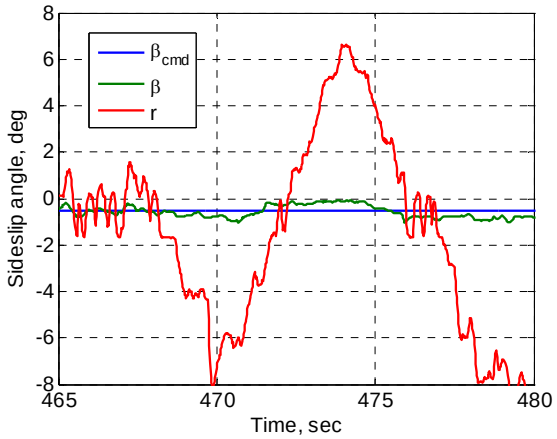

(f) Directional cross-coupling

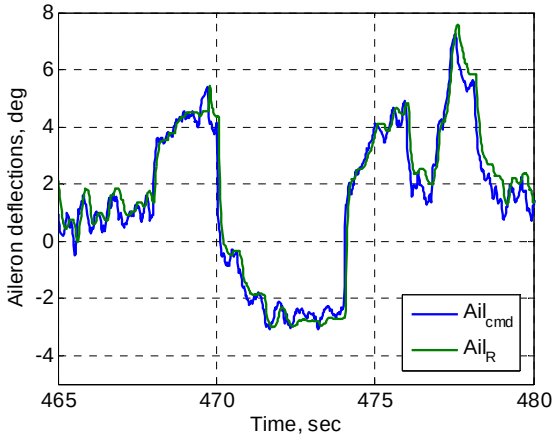

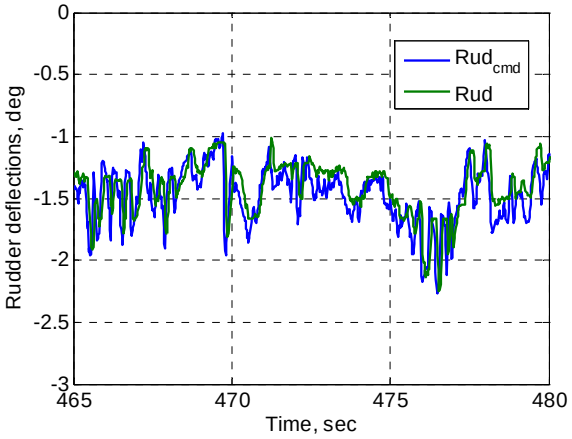

(g) Lateral-directional axes actuators

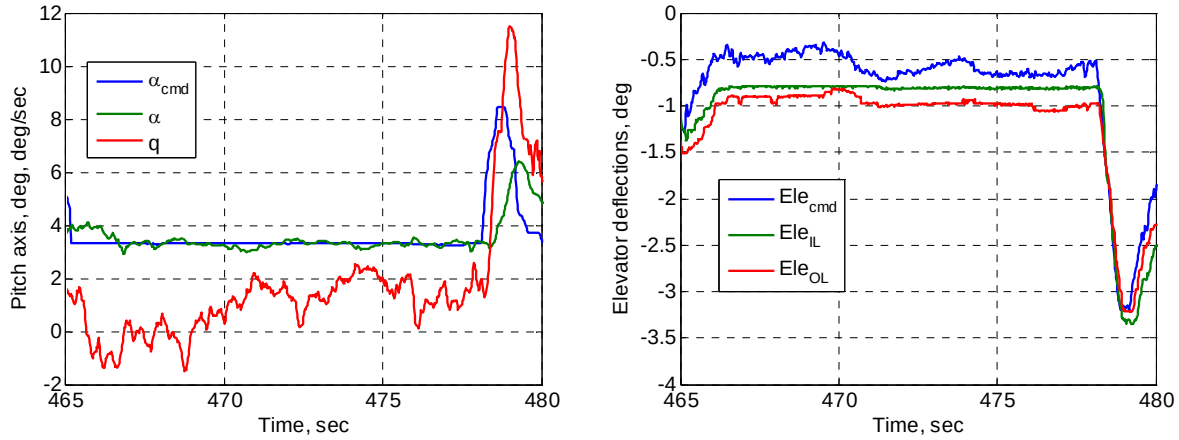

(h) Longitudinal cross-coupling (i) Longitudinal axis actuators

Figure 8. Nominal aircraft wave train injection response

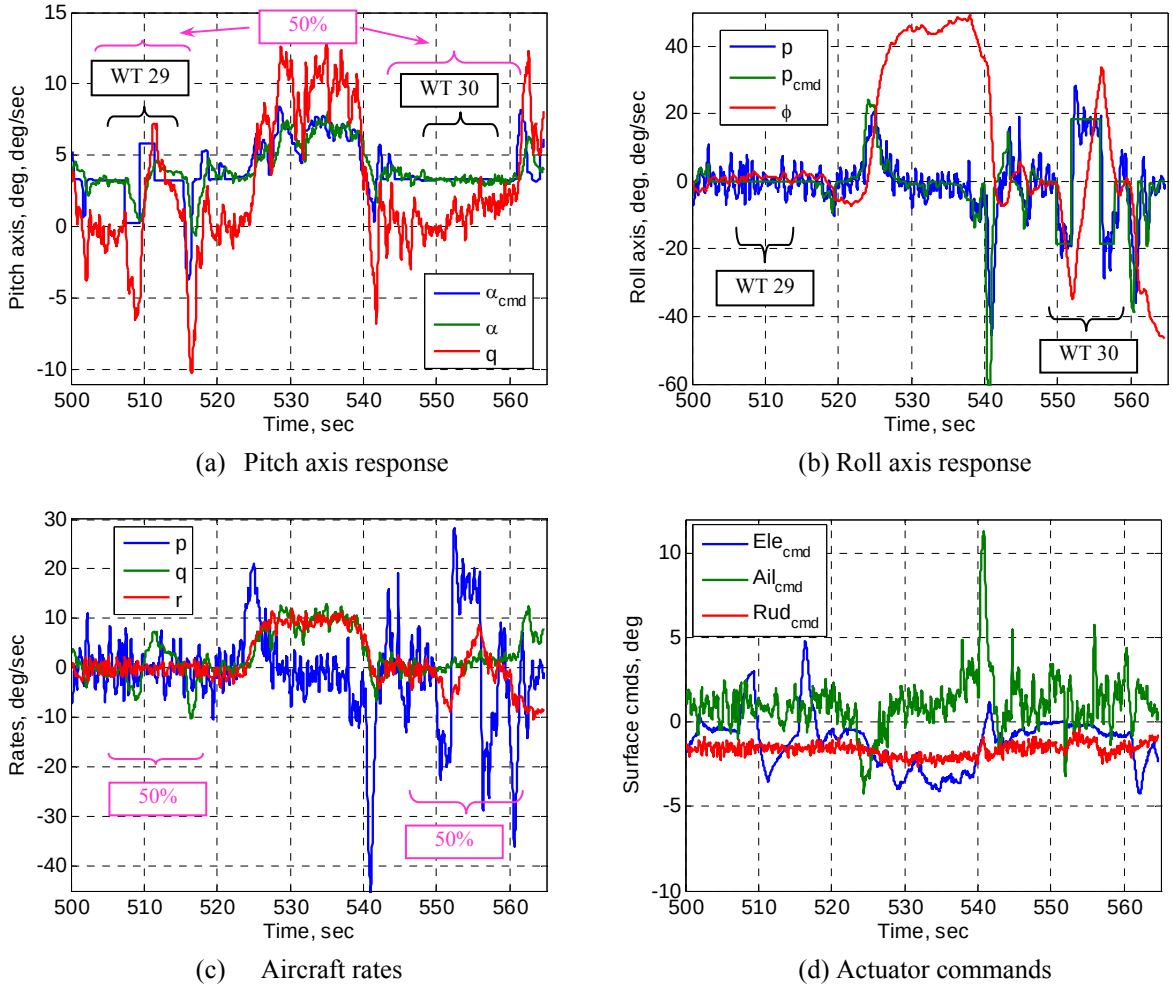

(a) Pitch axis response (b) Roll axis response

(c) Aircraft rates (d) Actuator commands

Figure 9. 50% Cmα/Clp stability degradation flight segment.

3. Task – 50% Cmα/Clp stability degradation

Following nominal aircraft pitch and roll axes wave trains, the aircraft stability is degraded in the following manner. The roll damping is reduced by scheduling spoilers as a function of roll rate to reduce Clp by 50% and the static longitudinal stability is reduced by reducing Cmα by 50%. The stability degradation fault is not carried through the turns, so the fault is engaged on the straight legs followed by a wave train. Fig. 9 shows roughly 65 second segment of flight covering 50% Cmα/Clp stability degradation. Plots in Fig. 9 (a)-(b) show pitch and roll axes response as well as mark where the 50% fault and wave trains were engaged. Fig. 9 (c)-(d) shows the angular rates and actuator commands respectively through the entire segment of flight.

The segments containing the 50% Cmα/Clp stability degradation fault and wave trains are isolated in Fig. 10. The time when the fault was engaged is shown on selected plots as a magenta finite time step. The engagement of fault, pitch axis wave train and associated state and actuator responses of interest are shown in Fig. 10 (a)-(d). Angle of attack and pitch rate response are very similar to that for the nominal aircraft (Fig. 8 (a)). However, notice the elevator response in Fig. 10 (b). The inboard elevator segment no longer follows the command; it is now scheduled with angle of attack, independent of the control law, to produce 50% reduction in Cmα. In the lateral-directional axes (Fig. 10 (c)), there is more excitation of the roll rate by turbulence, since roll damping is also 50% degraded, but not really an increase in cross coupling since the yaw rate response looks similar to the nominal case (Fig. 8 (b)).

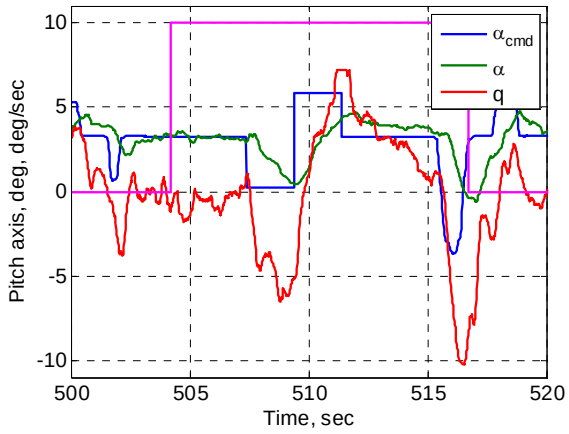

(a) Pitch axis wave train

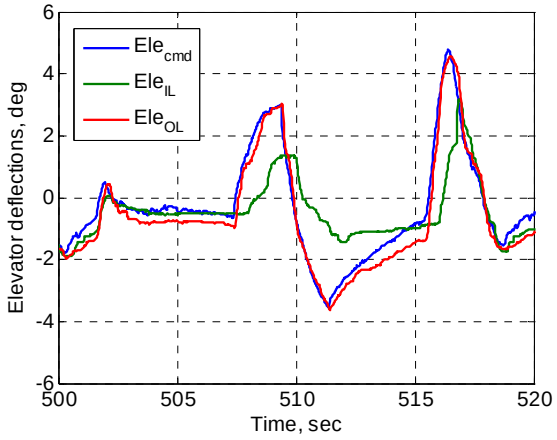

(b) Actuator deflections

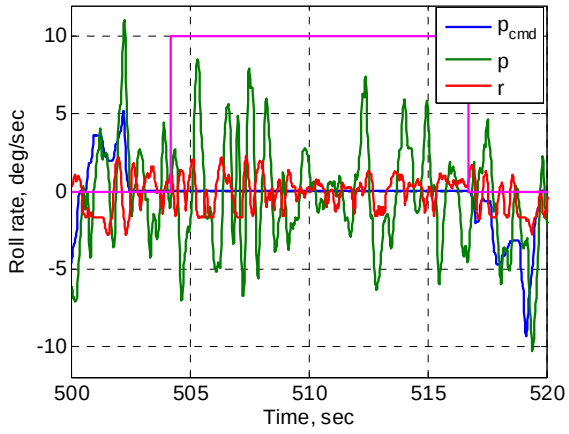

(c) Lateral-directional cross-coupling

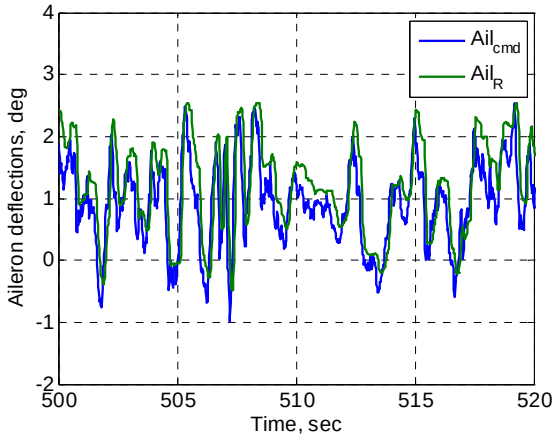

(d) Actuator deflections

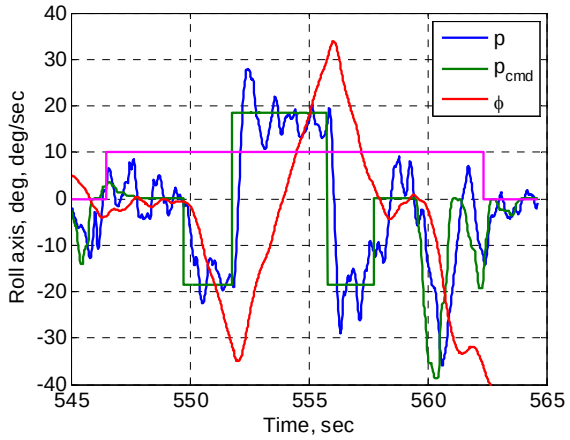

(e) Roll axis wave train

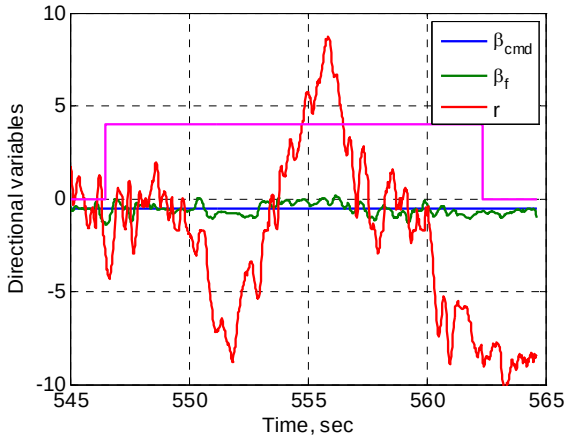

(f) Directional cross coupling

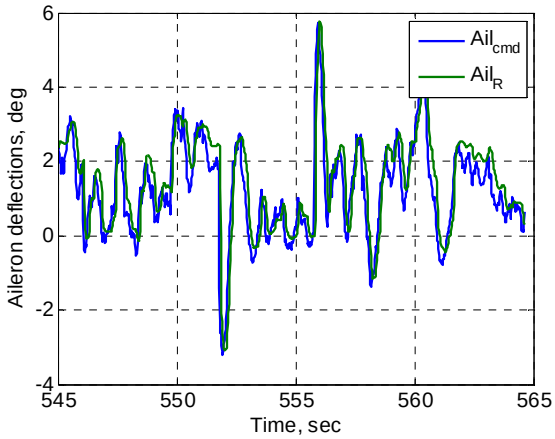

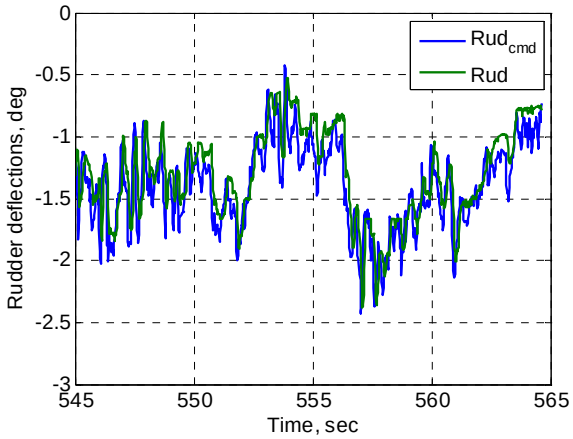

(g) Lateral-directional axes actuators

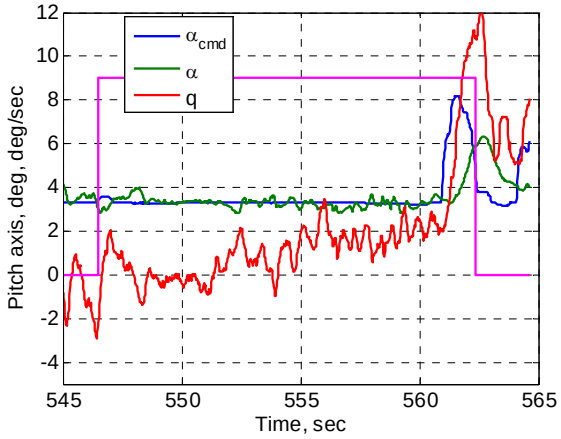

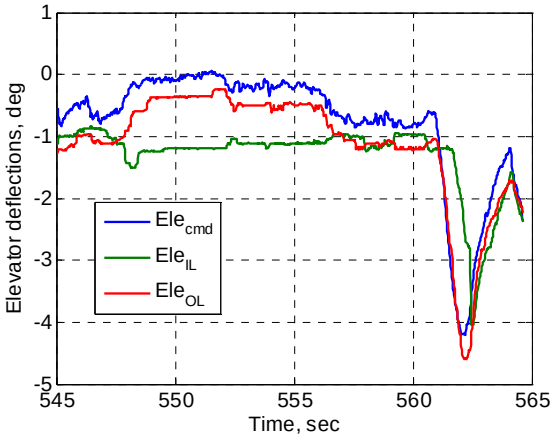

(h) Longitudinal cross coupling (i) Actuator deflections

Figure 10. 50% Cmα/Clp stability degradation wave train response.

The roll axes wave train and the associated variables are illustrated in Fig. 10 (e)-(i). As in the case with earlier engagement of 50% stability degradation fault, roll rate is slightly more excited by turbulence (Fig. 10 (e)) and the ailerons respond (Fig. 10 (g)) to quickly damp out any overshoot on the command and to cancel out the turbulence

induced uncommanded roll rate. It is also evident from the plot that the pilot initiated a turn while the fault was still engaged without any perceptible negative effect (at 560 sec). The directional axis cross-coupling is once again minimal (Fig. 10 (f)). The pitch axis cross-coupling (Fig. 10 (h)) is very similar to the nominal case (Fig. 8 (h)) and the elevator response once again shows inboard elevator destabilizing Cmα and not responding to control law commands (Fig. 10 (i)). Despite slightly increased response to turbulence by roll rate, the pilot's comment, interestingly enough, is that he did not detect any perceptible difference from the nominal aircraft.

4. Task - 75% Cmα/Clp stability degradation

Continuing with the next set of flight cards, the aircraft stability is degraded by 75% in Cmα/Clp using the same mechanism as described above. Plots in Fig. 11 (a)-(b) show pitch and roll axes response as well as mark where the 75% fault and wave trains were engaged. Fig. 11 (c)-(d) shows the angular rates and actuator commands respectively through the entire segment of flight.

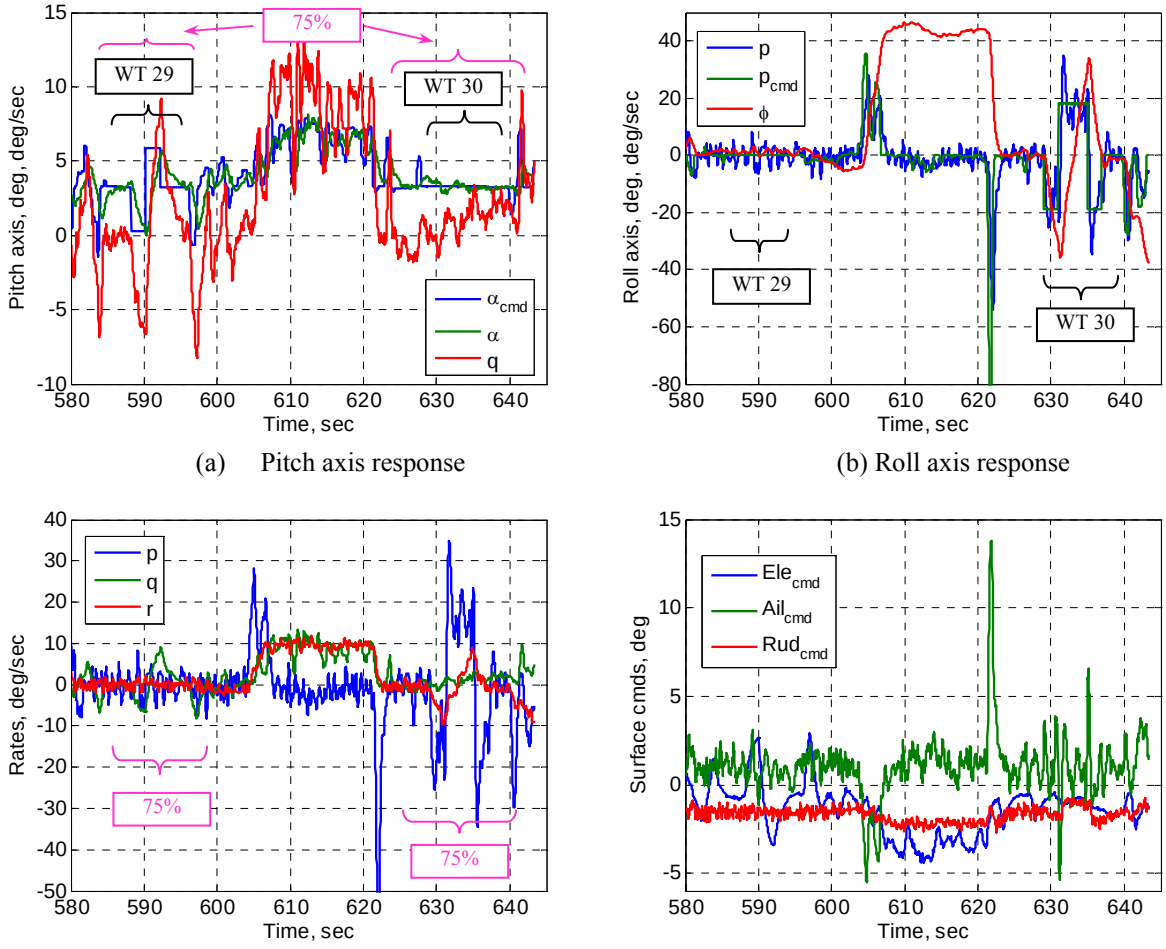

(a) Pitch axis response

(b) Roll axis response

(c) Aircraft rates

(d) Actuator commands

Figure 11. 75% Cmα/Clp stability degradation flight segment.

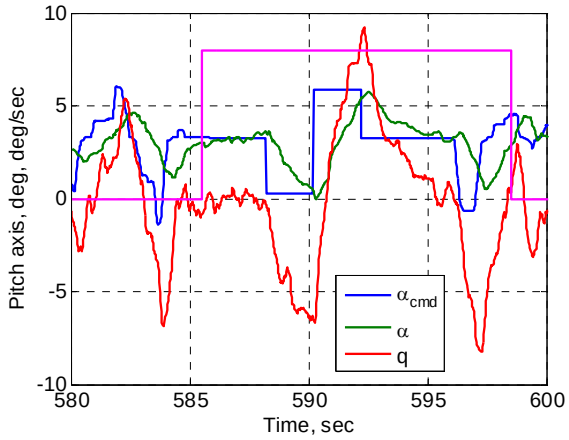

(a) Pitch axis wave train

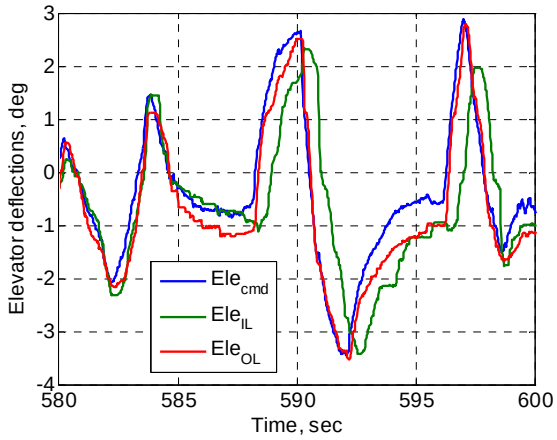

(b) Actuator deflections

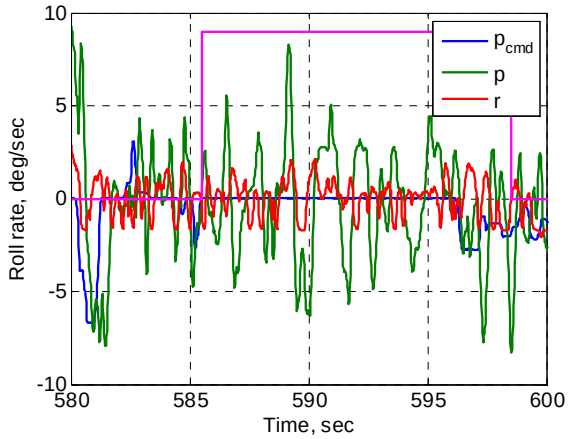

(c) Lateral-directional cross-coupling

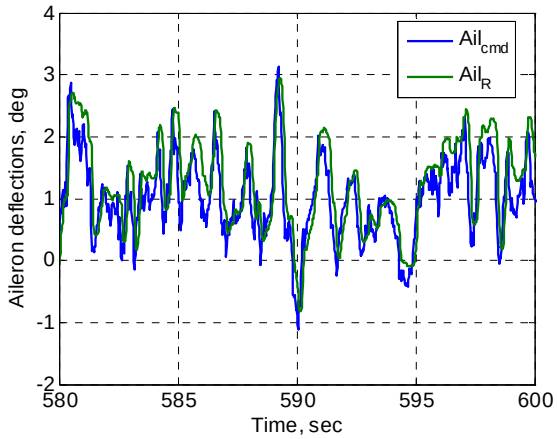

(d) Actuator deflections

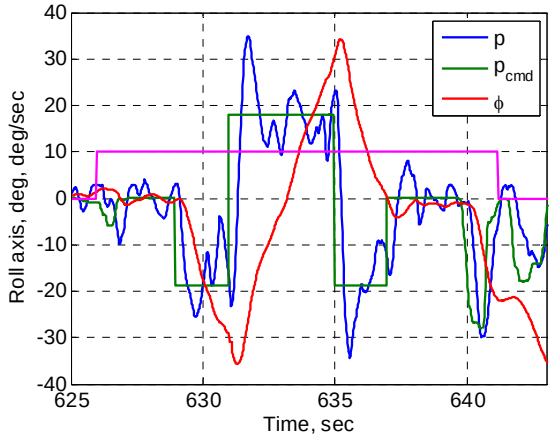

(e) Roll axis wave train

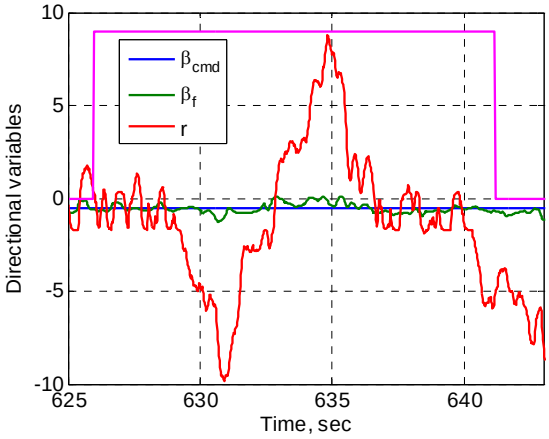

(f) Directional cross coupling

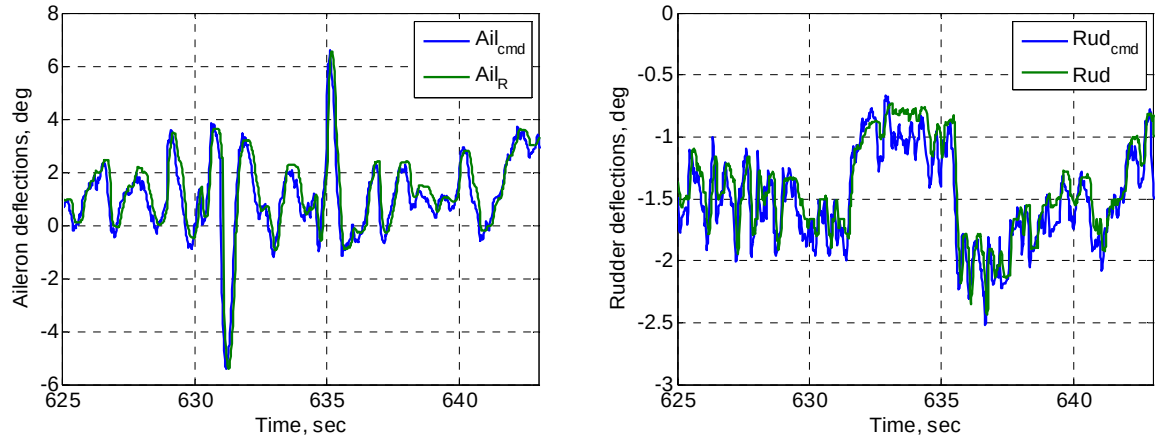

(g) Lateral-directional axes actuators

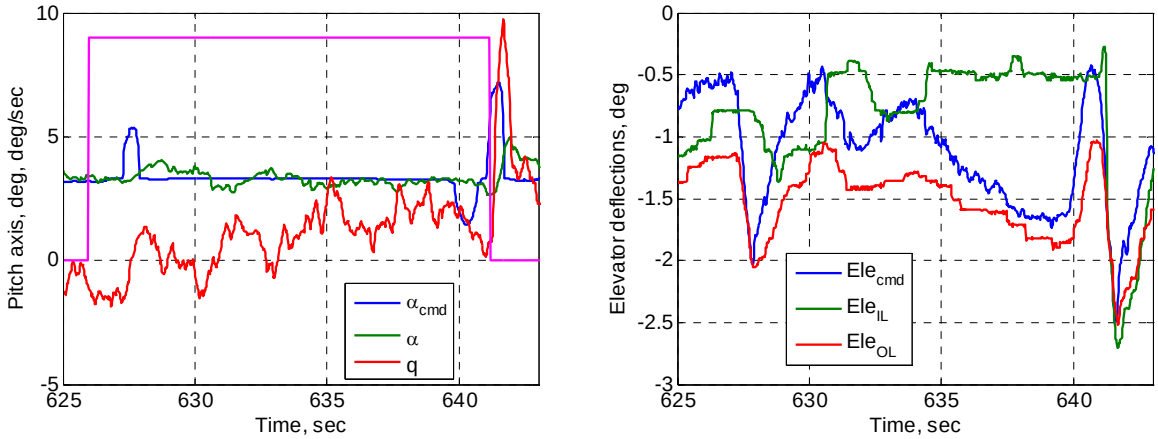

(h) Longitudinal cross coupling (i) Actuator deflections

Figure 12. 75% Cmα/Clp stability degradation wave train response.

The segments containing the 75% Cmα/Clp stability degradation fault and wave trains are isolated in Fig. 12. The time when the fault was engaged is shown on selected plots as a magenta finite time step. The engagement of fault, pitch axis wave train and associated state and actuator responses of interest are shown in Fig. 12 (a)-(d). Angle of attack and pitch rate response are very similar to that for the nominal aircraft (Fig. 8 (a)). In the lateral-directional axes (Fig. 12 (c)), there is more excitation of the roll rate by turbulence, since roll damping is also 75% degraded, but not really an increase in cross coupling since the yaw rate response looks similar to the nominal case (Fig. 8 (b)).

The roll axes wave train and the associated variables are illustrated in Fig. 12 (e)-(i). As is the case with earlier engagement of 75% stability degradation fault, roll rate is slightly more excited by turbulence (Fig. 12 (e)) and the ailerons respond (Fig. 12 (g)) to quickly damp out any overshoot on the command and to cancel out the turbulence induced uncommanded roll rate. Once again the pilot initiated a turn while the fault was still engaged (at 641 sec) without any perceptible negative effect. The directional axis cross-coupling is once again minimal (Fig. 12 (f)). The pitch axis cross-coupling (Fig. 12 (h)) is very similar to the nominal case (Fig. 8 (h)) and the elevator response once again shows inboard elevator destabilizing Cmα and not responding to control law commands (Fig. 12 (i)). Stability degradation in a cross axis, in of itself does not increase cross-coupling; however, any roll rate excitation by a pitch axis command will be less damped for a degraded Clp and will require more effort by the controller to eliminate. There were no pilot comments for this stability degradation fault.

5. Task - 100% Cmα/Clp stability degradation – neutrally stable aircraft

This next set of maneuvers was performed with a neutrally stable aircraft and 50% degradation in pitch control power, i.e. 100% degradation in Cmα/Clp generated by changes in inboard elevator segments and spoilers. Again, the fault was engaged only on a straight leg followed by a wave train being engaged, then the fault was disengaged after the wave train was completed.

Plots in Fig. 13 (a)-(b) show pitch and roll axes response as well as mark where the 100% fault and wave trains were engaged. Fig. 13 (c)-(d) shows the angular rates and actuator commands respectively through the entire segment of flight. The deterioration in dynamic response, especially in roll rate, compared to that of the nominal aircraft becomes apparent as well as increased actuator amplitudes in an attempt to compensate.

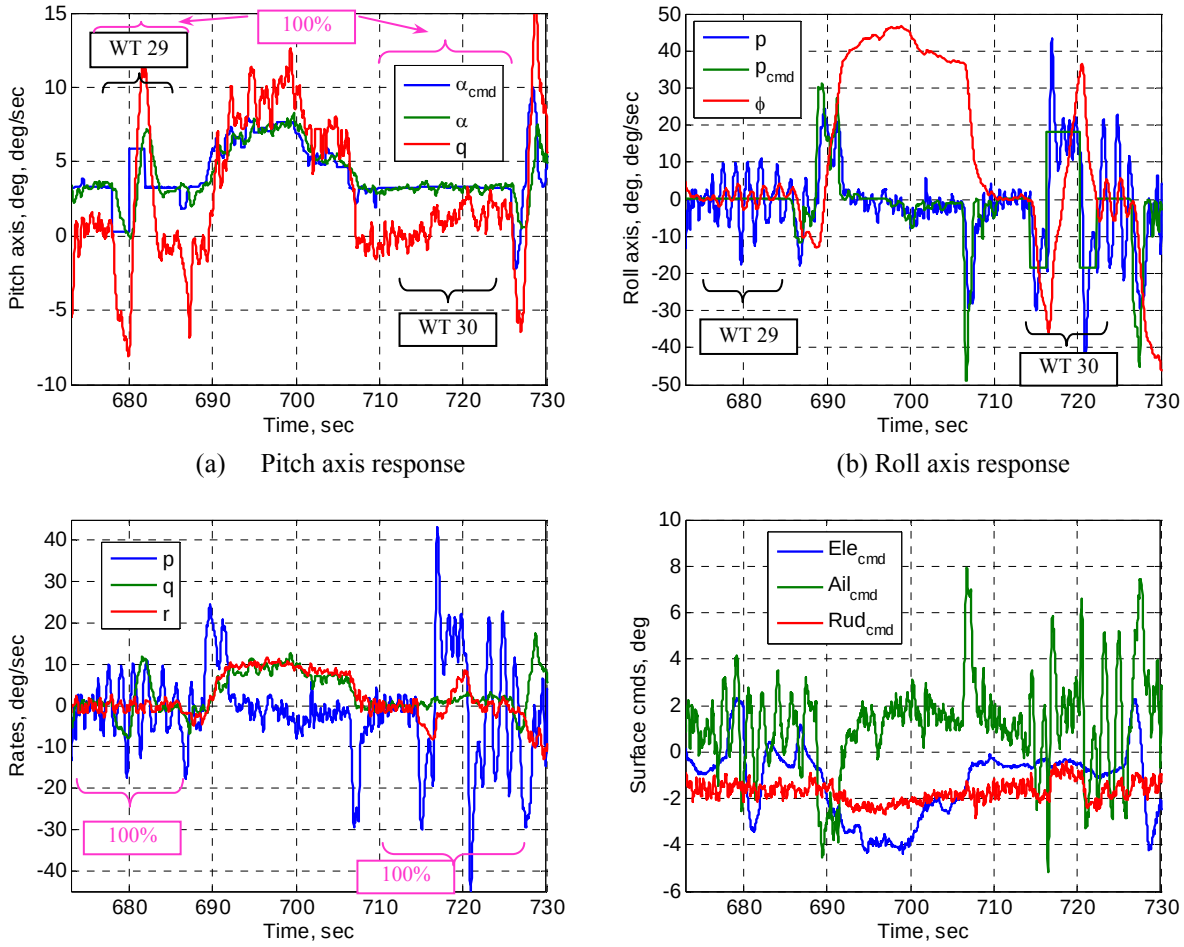

(a) Pitch axis response

(b) Roll axis response

(c) Aircraft rates

(d) Actuator commands

Figure 13. 100% Cmα/Clp stability degradation flight segment – neutrally stable aircraft.

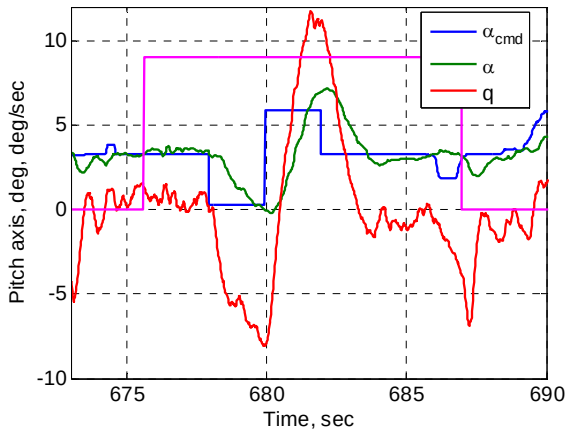

(a) Pitch axis wave train

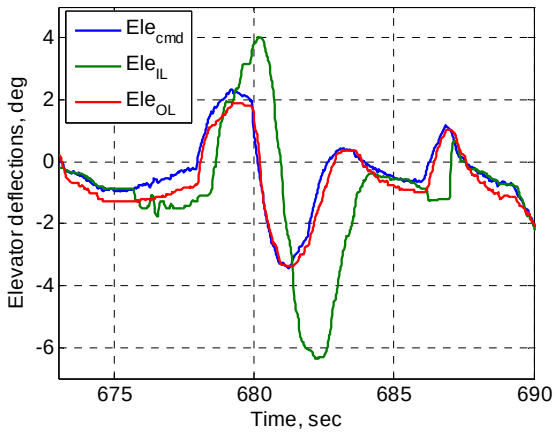

(b) Actuator deflections

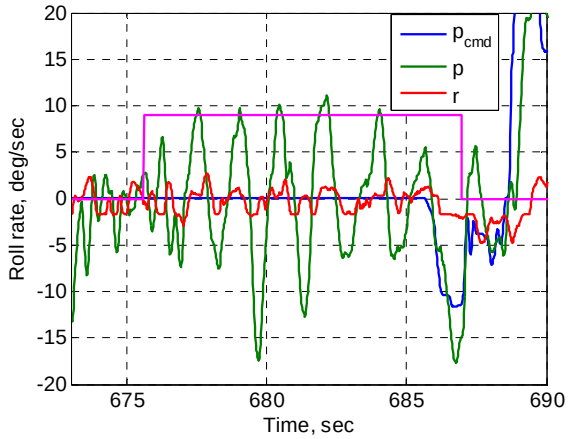

(c) Lateral-directional cross-coupling

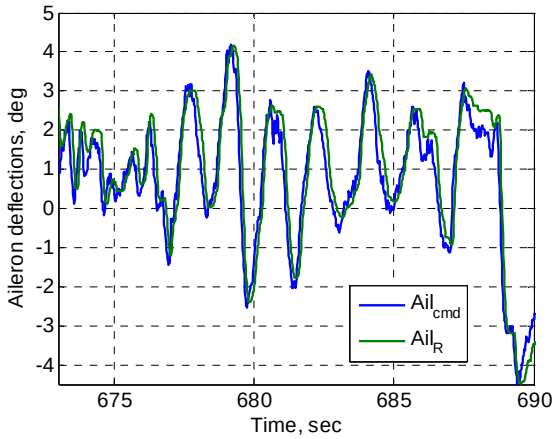

(d) Actuator deflections

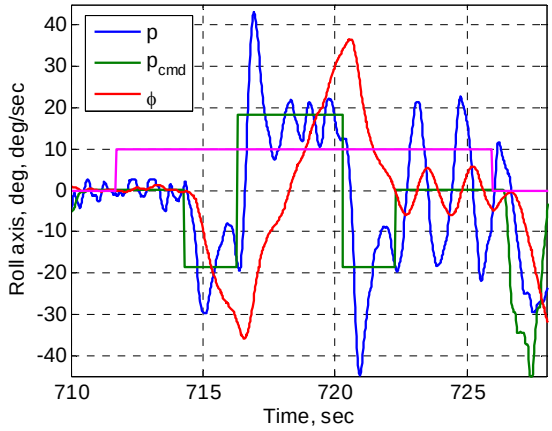

(e) Roll axis wave train

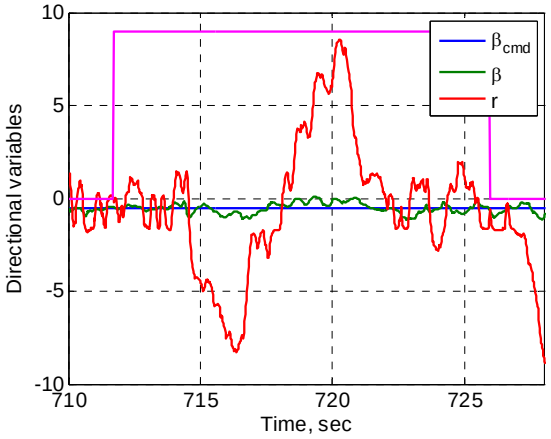

(f) Directional cross coupling

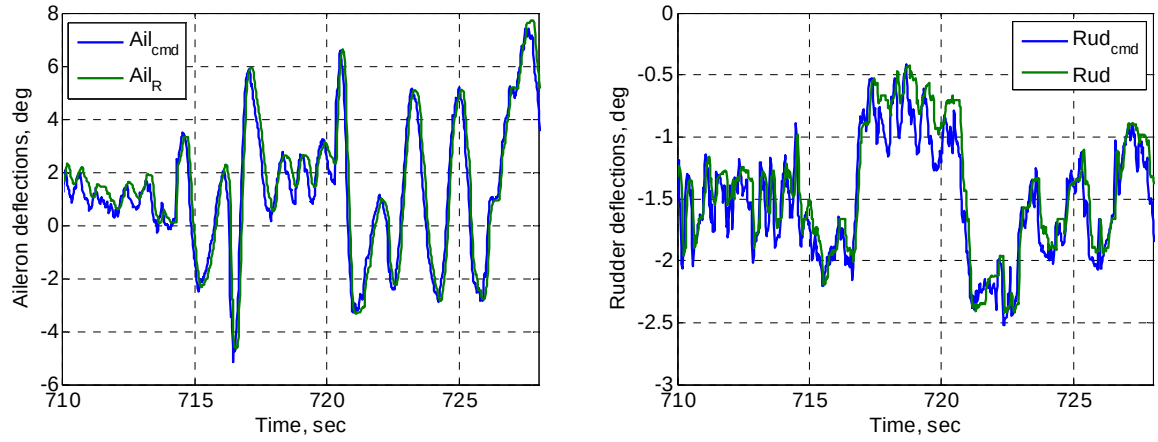

(g) Lateral-directional axes actuators

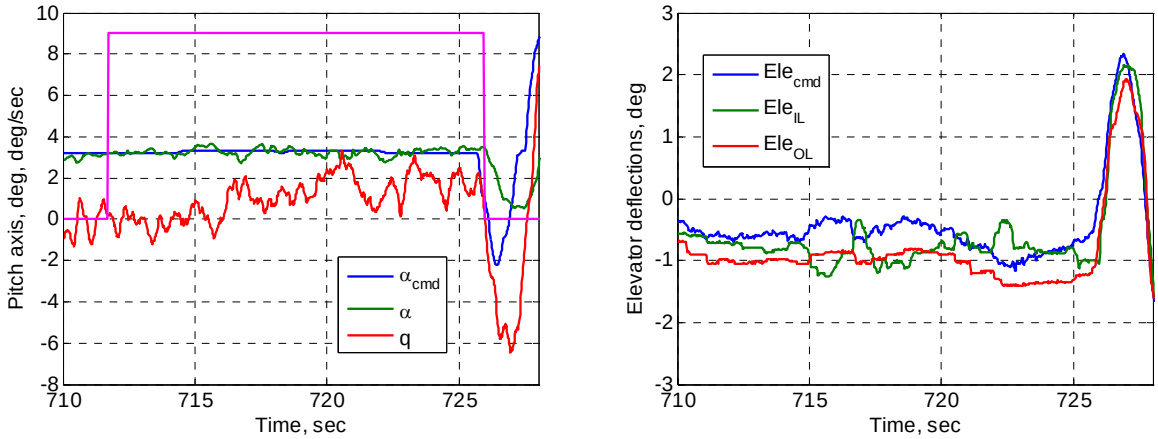

(h) Longitudinal cross coupling (i) Actuator deflections

Figure 14. 100% Cmα/Clp stability degradation wave train response.

The segments containing the 100% Cmα/Clp stability degradation fault and wave trains are isolated in Fig. 14. The time when the fault was engaged is shown on selected plots as a magenta finite time step. The engagement of fault, pitch axis wave train and associated state and actuator responses of interest are shown in Fig. 14 (a)-(d). The overall pitch axis closed loop damping has decreased as evidenced by an overshoot in angle of attack response and larger magnitude pitch rate response. The inboard elevator segment in Fig. 14 (b), scheduled with angle of attack independent of the control law, has relatively large deflections to produce 100% reduction in Cmα. In the lateral-directional axes (Fig. 14 (c)), there is more excitation of the roll rate by turbulence, since roll damping is also 100% degraded, and potentially more cross-coupling in the roll axis. The yaw rate response still looks similar to the nominal case (Fig. 8 (b)) and remains within ±5 deg/sec. The pilot did comment that he observed roll ratcheting during the pitch axis wave train.

The roll axes wave train and the associated variables are illustrated in Fig. 14 (e)-(i). For a 100% stability degradation fault, roll rate is more oscillatory, excited by turbulence and stick inputs (Fig. 14 (e)) and the ailerons respond (Fig. 14 (g)) to try to damp out any overshoot and turbulence induced oscillations. However, at the tail end of the wave train, there are two ±20 deg/sec oscillations that the controller is slow in damping out. Perhaps at this stage the controller is reaching its ability to provide robust performance in the roll axis. The rudder response in this case also has a more distinctive shape but still small amplitude as it tries to help control roll rate without exciting

yaw rate and sideslip, which is commanded to 0 at all times. The directional axis cross-coupling is once again minimal, ±10 deg/sec (Fig. 14 (f)). The pitch axis cross-coupling (Fig. 14 (h)) is once again very similar to the nominal case (Fig. 8 (h)) and the elevator response once again shows inboard elevator destabilizing Cmα and not responding to control law commands (Fig. 14 (i)). The pilot observed that there was no observable roll ratcheting during the roll rate doublet unlike what he saw during the pitch axis doublet.

6. Task - 125% Cmα/Clp stability degradation – unstable aircraft

The final segment in stability degradation was to change the aircraft dynamics to highly unstable in pitch and roll axes achieved by degrading Cmα/Clp 125% with the standard 50% reduction in pitch axis control power. Plots in Fig. 15 (a)-(b) show pitch and roll axes response as well as mark where the 125% fault was engaged. Fig. 15 (c)-(d) shows the angular rates and actuator commands respectively through the entire segment of flight. The controller was able to handle unstable pitch axis as evidenced from Fig. 15 (a) but clearly could not handle the excitation of roll rate (Fig. 15 (b)).

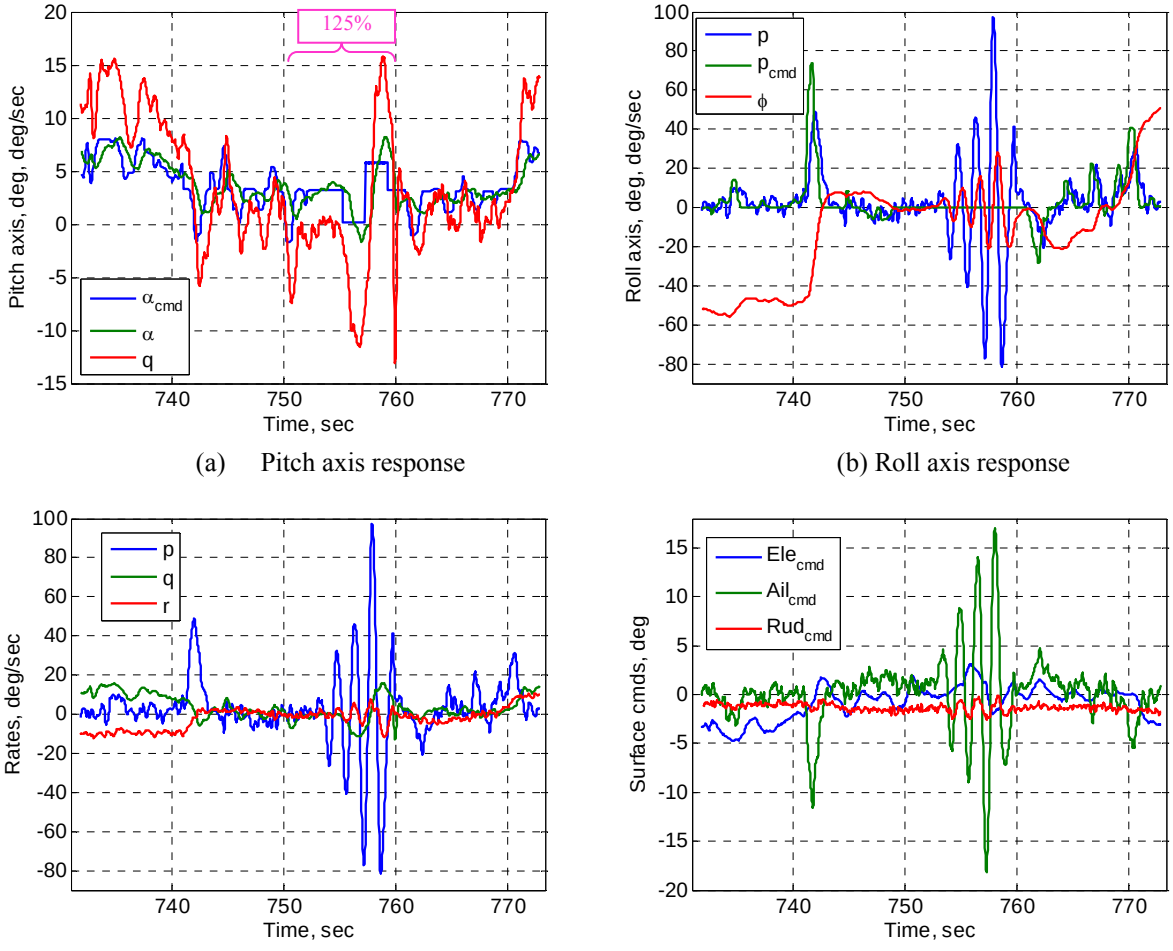

(a) Pitch axis response

(b) Roll axis response

(c) Aircraft rates

(d) Actuator commands

Figure 15. 125% Cmα/Clp stability degradation flight segment – unstable aircraft.

Detailed representation of the fault and pitch axis wave train are plotted in Fig. 16 (a)-(d). The angle of attack doublet further excited diverging roll rate oscillations and the pilot called "knock it off" (KIO), a signal for abandoning a particular maneuver/fault. Note that even though the pilot called "knock it off" he did not abandon the

control law. The test engineer simply flipped the switch to turn off the stability degradation fault and the controller recovered its nominal performance immediately. The pilot proceeded to fly into a typical aggressive turn less than 10 seconds after the fault was terminated, around 770 seconds (Fig. 15 (a)-(b)). Note an immediate roll rate recovery as soon as the fault was disengaged, illustrated in Fig. 16 (h), at around 760 seconds. In addition, from Fig. 16 (e) notice that the pitch axis wave train continues for about 1 second without any additional input from the pilot after the fault was disengaged. The fault disengagement causes an abrupt transient in pitch rate that the controller damps out very quickly before the pilot reengaged with the aircraft. The pilot reengaged at 761 seconds and tried to counteract the roll but quickly realized that the controller has returned the aircraft to nominal performance and he returned the lateral stick to neutral by 765 seconds before proceeding with a typical turn. For the robustness vs. performance tradeoffs made in the design, this particular L_1 all-adaptive controller could not provide stable response in the pitch axis for a highly unstable aircraft.

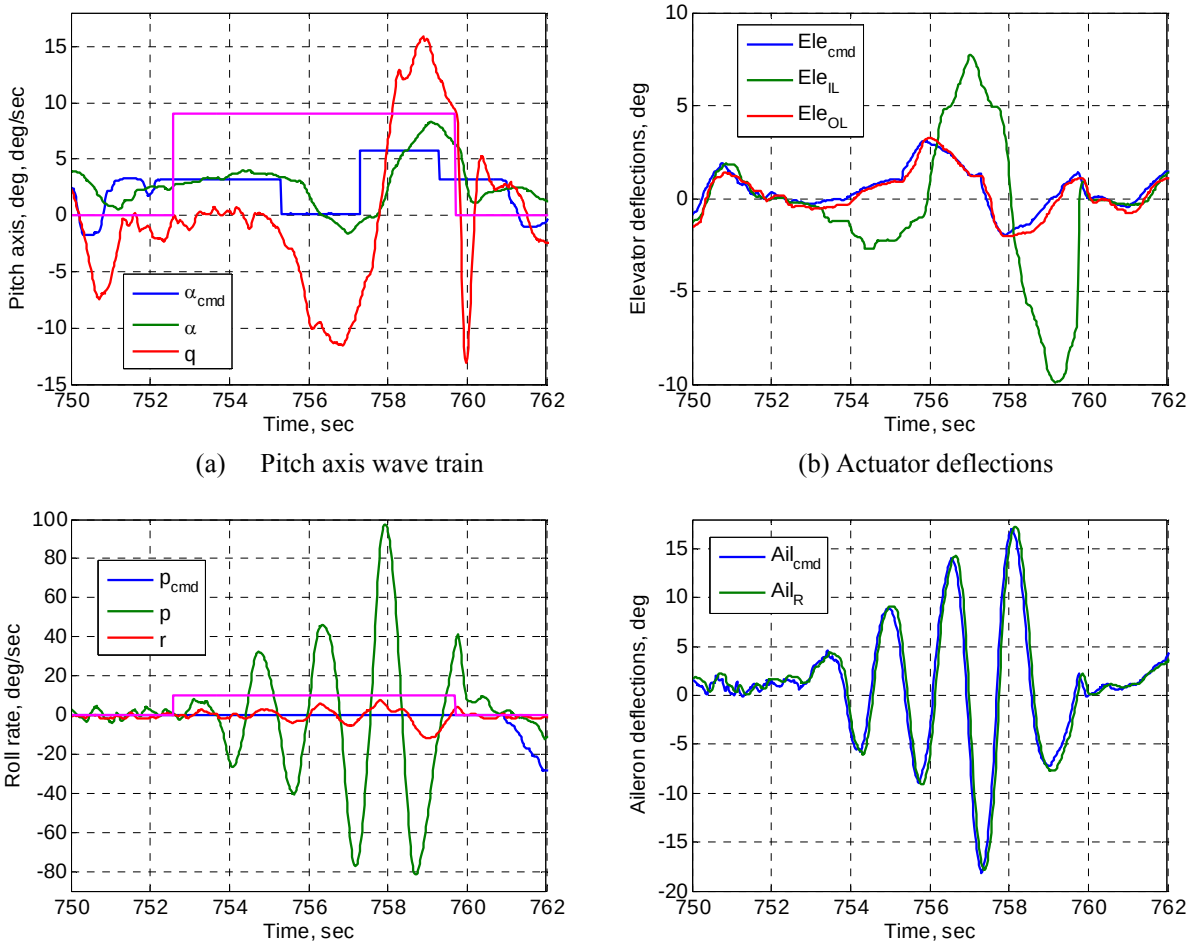

(a) Pitch axis wave train

(b) Actuator deflections

(c) Lateral-directional cross-coupling

(d) Actuator deflections

Figure 16. 125% Cmα/Clp stability degradation wave train response.

B. High angle of attack and post-stall operations

Interest in post-stall high angle of attack conditions during June 2010 flight test were two fold. First, there was an interest in exploiting the AirSTAR capability as a flying wind tunnel to model unsteady nonlinear aerodynamics encountered at high angles of attack post-stall flight regimes. The second impetus came from trying to stress the L_1

all-adaptive flight control law and further explore its performance under flight conditions far removed from the original design point. Flight test description relevant to post-stall angle of attack operations is given below[30]. Since this was a first foray into angles of attack well past the stall condition, the rules under which the maneuvers were to be abandoned were on a conservative side. The rules applied equally to the open loop stick-to-surface as well as to an L_1 research control law high angle of attack acquisition.

Angle of Attack Buildup[30]

The primary purpose of this buildup was to investigate the feasibility of attaining a post-stall equilibrium flight condition from which small amplitude pre-programmed perturbation inputs can be superimposed on the pilot's commands. The primary challenge associated with this buildup was expected to be roll-off due to asymmetric wing stall. Various entry techniques were to be investigated. This included variation of entry rate, target alpha, and lateral / directional control inputs as needed to attain a stable post-stall flight condition.

To reach the desired post-stall angle of attack, the aircraft must go through stall which is characterized as follows. Roll asymmetry with strong roll-off tendency was expected to occur at about 13 deg angle of attack. Also, roll damping characteristics were expected to rapidly change from stable to slightly unstable in the 10 deg to 12 deg angle of attack range. At angles of attack above stall, roll damping was expected to improve and aerodynamic asymmetry was expected to reduce. The defining stall characteristic was expected to be an unstable pitch break occurring at 13 deg angle of attack. Low static and dynamic longitudinal stability was expected at 15 deg angle of attack.

The maneuver was to be abandoned if bank angle exceeded 45 deg, angle of attack exceeded 30 deg, or the aircraft descended below 900 feet AGL.

High Angle Of Attack Capture Using An Adaptive FCL[30]

The mode 3.6 FCL [L1 all-adaptive control law] was to be used to capture a post-stall angle of attack, anywhere between 15 deg and 20 deg according to the flight card[31]. The purpose was to evaluate the control law's ability to adapt to the natural degradation (from nominal design conditions) of the airplane's stability and control characteristics.

The high angle of attack capture with an L_1 all-adaptive control law was performed as the last set of maneuvers on flight 23 (see Fig. 5). The pilot acquired α=18 deg. twice in a very repeatable manner. His comment was that the aircraft appeared to want to go to α=18 deg. and stay there. In addition, the aircraft was very well behaved in roll during the entire acquisition maneuver. Moreover, the control law was very predictable. Two flights later on the same morning, flight 25, the same high angle of attack acquisition maneuver was attempted using stick to surface control, nominal control for the aircraft, as described in angle of attack buildup above. As a point of reference, the GTM is open loop Level 1 FQ aircraft in its normal flight envelope. The pilot made 3 attempts to capture 18 degrees angle of attack without exceeding 45 degrees of bank angle, none of these were successful. Figs. 17 - 20 show a number of variables of interest for post-stall angle of attack maneuvers and provide side-by-side look at the performance of an L_1 all-adaptive control law and stick-to-surface control. Fig. 17 shows the angle of attack, roll rate and bank angle as a function of time as the pilot made his first attempt to capture α=18 deg. The largest roll rate with an L_1 controller encountered between 13 and 14 degrees was less than ± 20, which translated to roughly 12 degrees bank angle. The bank angle excursion lasted for less than 2 seconds before returning to a fairly constant 5 degree offset. The pilot captured and maintained 18 degrees angle of attack for over 7 seconds. Moreover, the combination of power setting and pilot command saturated the elevator (all segments) from 849 to 854 seconds without any observable ill effect on the control system or aircraft dynamics (Fig. 17 (c)). At 854 seconds the pilot initiated recovery, recovered by 856 seconds and initiated a turn by 858 seconds. The responses for stick to surface are self-explanatory in Fig. 17 (a).

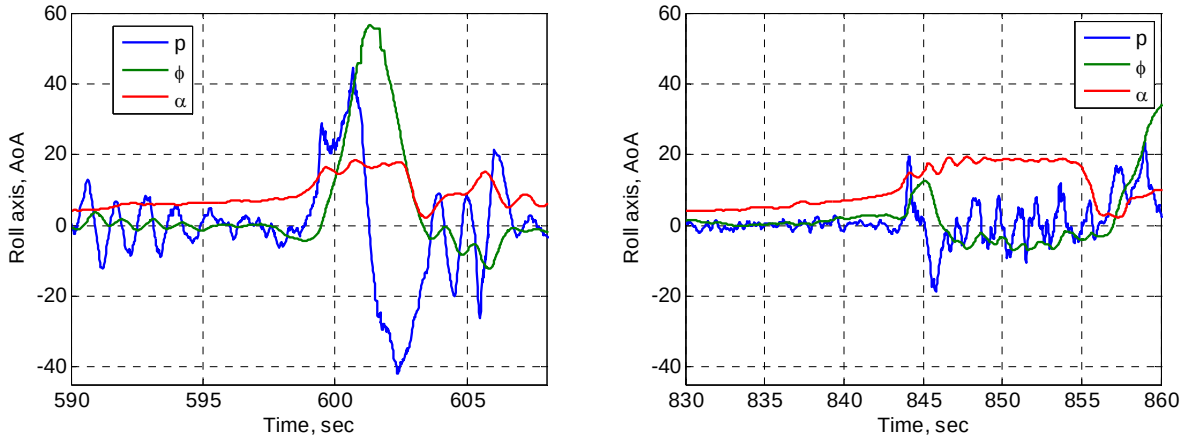

(a) Stick-to-surface (b) L_1 all-adaptive controller

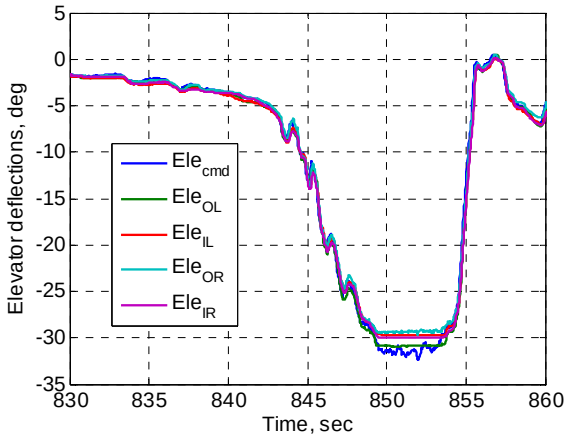

(c) Elevator surface response for L_1 all-adaptive controller

Figure 17. Post stall angle of attack capture maneuver defining variables – angle of attack (α), roll rate (p) and bank angle (ϕ).

Fig. 18 shows the typical α-β envelope. Each one of the attempted angle of attack captures is shown in their respective plots. For an L_1 all-adaptive control law sideslip angle is $-2 \le \beta < 1$ while for stick to surface sideslip is $-2 < \beta < 6.5$. More dramatic differences in performance are observed in the variables that are explicitly affected by high angle of attack aerodynamics. In particular the roll rate that translates into bank angle. Fig. 19 shows the α-p envelope and the performance of stick to surface and L_1 adaptive controller respectively. Note that an L_1 controller roll rate never exceeds 20 deg/sec while in state to surface configuration roll rate exceeds 40 deg/sec in the best case scenario, acquisition attempt 3. Persistently high roll rate necessarily translates into large bank angles as is shown in Fig. 20 (a). Under admittedly conservative rules for allowable bank angle for this maneuver, all three stick to surface attempts had to be abandoned since each exceeded 45 degrees bank angle. Bank angle under L_1 all-adaptive control law, however, never exceeded 15 degrees, Fig. 20. Clearly an L_1 all-adaptive controller significantly improved pilot's ability to fly the aircraft at high angles of attack. The controller, designed at a single flight condition with desired dynamics to match (80 KEAS, α~4.5 deg), has provided some increase in pitch damping and significant increase in roll rate damping through stall and post-stall pitch break and roll-off. Moreover, an L_1 all-adaptive controller demonstrated robustness to persistently saturated actuators at high angle of attack. A detailed analysis of

the stability and performance of the L_1 adaptive controller in the presence of control input saturation can be found in Ref. 32 .

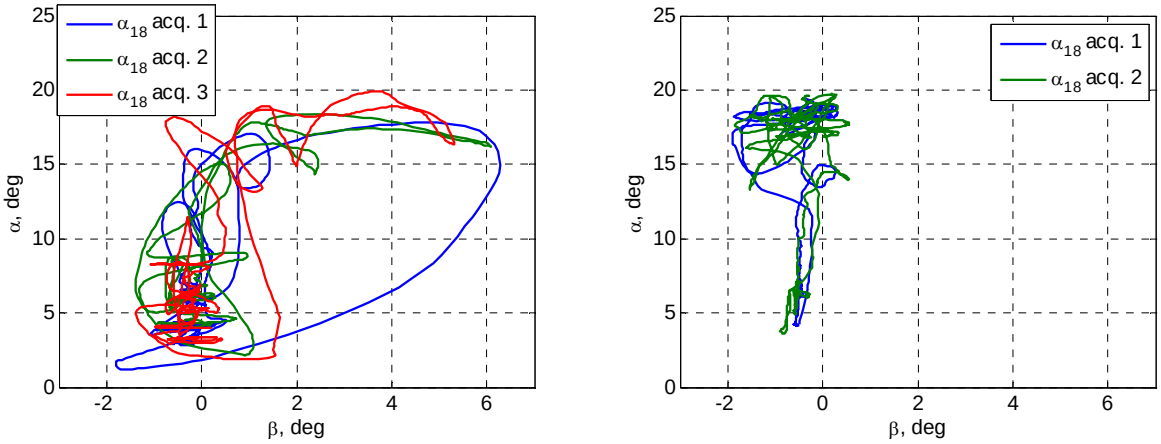

(a) Stick-to-surface (b) L_1 all-adaptive controller

Figure 18. Post stall angle of attack capture – angle of attack (α) vs. sideslip angle (β) envelope.

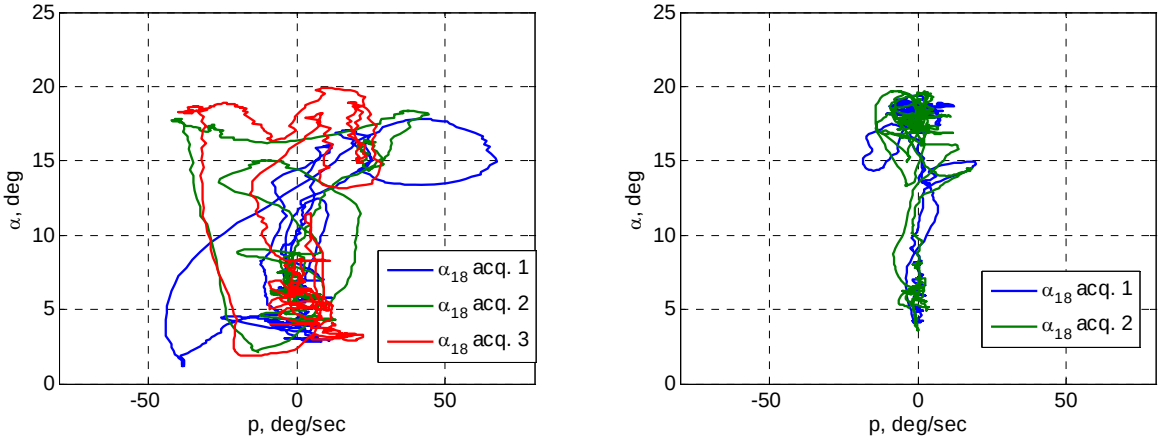

(a) Stick-to-surface (b) L1 all-adaptive controller

Figure 19. Post stall angle of attack capture – angle of attack (α) vs. roll rate (p) envelope.

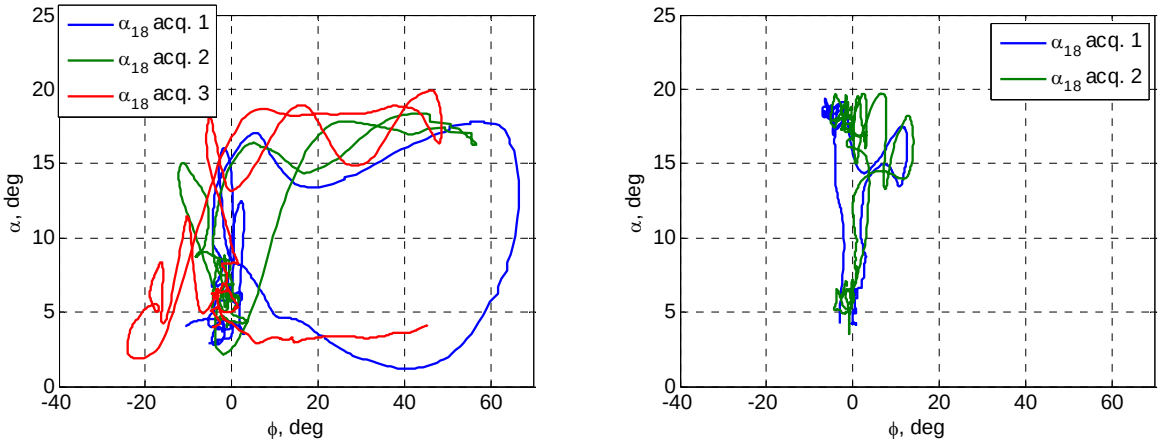

(a) Stick-to-surface (b) L1 all-adaptive controller

Figure 20. Post stall angle of attack capture – angle of attack (α) vs. bank angle (ϕ) envelope.

V. Conclusions / Future Plans

Flight test results of an L_1 all-adaptive control law flown on the NASA Langley's AirSTAR GTM twin jet engine dynamically scaled aircraft have been discussed. The purpose behind an all-adaptive control law was to stress the methodology to better understand not only its practical performance but also its behavior at the limits with no contribution from a baseline controller. The design and tuning of an L_1 all-adaptive control law to achieve Level 1 flying qualities and the classical tradeoff between robustness to system latency vs. performance under significant nonlinear cross-coupling was found to be consistent with the theory. The control laws were designed to attain one set of desired dynamics specified at 80KEAS and 4.5 deg. angle of attack wings level equilibrium flight. As a point of reference, the GTM is open loop Level 1 FQ aircraft. With this set of desired dynamics the control law was robust to 0.125 seconds of additional time delay and was able to track angle of attack and roll rate doublets in the presence of stability degradation, expressed as degradation in $C_{m\alpha}/C_{lp}$, all the way to a neutrally stable aircraft. Moreover, the same control law was applied to a post-stall high angle of attack regime to capture and hold high angle of attack. The controller provided some increase in pitch damping as well as significant increase in roll damping through stall and post-stall pitch break and roll-off phenomena. Thus, an L_1 all-adaptive controller significantly improved pilot's ability to fly the aircraft at high angles of attack and decreased his workload.

Future work will include improved design in post-stall angle of attack region to support precision tracking of different inputs required by nonlinear aerodynamic modeling work. Additional work will include designing a baseline controller and augmenting the current L_1 architecture in order to explore precisely the advantages and disadvantages of all-adaptive vs. baseline-augmenting implementations.

VI. Acknowledgments

The authors would like to express their deep gratitude to the staff of the AirSTAR Flight Test Facility for their support with control law implementation, their insights into flight dynamics and piloted evaluations. There are too many individuals who deserve recognition to mention by name; however, we would like to single out a few for special thanks: Kevin Cunningham who not only serves as the PI for the AirSTAR and the first evaluation gateway through which all research control laws must pass, but who has also offered valuable advice every step of the way as the authors designed their first flight control law that had to fly with a pilot in the loop on an aircraft with challenging dynamics; Dan Murri, who serves as the research pilot and whose word on flyability is final, for his patience while the authors tried to translate his comments into which control variables needed to be changed; and, John "Mike' Cronauer, who serves as one of the software experts on the project, for exercising his flying skills as a former F18 pilot to stress the control laws and take them well beyond the allowable research envelope.

This control law design experience has made us all better researchers and for that we are especially grateful.

VII. References

[1] Cunningham K., Foster J. V., Morelli E. A., and Murch A. M., "Practical Application of a Subscale Transport Aircraft for Flight Research in Control Upset and Failure Conditions," AIAA 2008-6200, AIAA Atmospheric Flight Mechanics Conference, Honolulu, HI, 2008.

[2] Murch, A. M., "A Flight Control System Architecture for the NASA AirSTAR Flight Test Infrastructure," AIAA 2008-6990, AIAA Guidance, Navigation, and Control Conference and Exhibit, Honolulu, HI, 2008.

[3] Murch, A. M., Cox, D.E, Cunningham K.," Software Considerations for Subscale Flight Testing of Experimental Control Laws," AIAA InfoTech@Aerospace, Seattle, WA, April, 2009.

[4] Jordan, T. L., Foster, J. V., Bailey, R. M., and Belcastro, C. M., "AirSTAR: A UAV Platform for Flight Dynamics and Control System Testing,", AIAA 2006-3307, 25th AIAA Aerodynamic Measurement Technology and Ground Testing Conference, San Francisco, CA, 2006.

[5] Jordan, T. L., Langford, W. M., and Hill, J. S., "Airborne Subscale Transport Aircraft Research Testbed – Aircraft Model Development," AIAA 2005-6432, AIAA Guidance, Navigation, and Control Conference, San Francisco, CA, 2005.

[6] Bailey, R.M., Hostetler, R.W., Barnes, K.N., Belcastro, Christine M., and Belcastro, Celeste M., "Experimental Validation: Subscale Aircraft Ground Facilities and Integrated Test Capability," AIAA 2005-6433, AIAA Guidance, Navigation, and Control Conference, San Francisco, CA, 2005.

[7] Foster, J. V., K. Cunningham, C. M. Fremaux, G. Shah, E. Stewart, R. Rivers, J. Wilborn, and W. Gato, "Dynamics Modeling and Simulation of Large Transport Airplanes in Upset Conditions, AIAA-2005-5933, AIAA Guidance, Navigation, and Control Conference, San Francisco, CA, August 2005.

[8] Xargay, E., Hovakimyan, N. and C. Cao, "L_1 Adaptive Controller for Multi-Input Multi-Output Systems in the Presence of Nonlinear Unmatched Uncertainties," American Control Conference, June 2010, Baltimore, MD, pp. 875-879.

[9] Cao, C. and N. Hovakimyan, L_1 Adaptive Controller for Systems with Unknown Time-varying Parameters and Disturbances in the Presence of Non-zero Trajectory Initialization Error, International Journal of Control, vol. 81, No. 7, pp. 1148-1162, 2008.

[10] Cao, C. and N. Hovakimyan, L_1 Adaptive Output Feedback Controller for Systems of Unknown Dimension, IEEE Transactions on Automatic Control, vol. 53, No. 3, pp. 815-821, 2008.

[11] Cao, C. and N. Hovakimyan, Design and Analysis of a Novel L_1 Adaptive Control Architecture with Guaranteed Transient Performance, IEEE Transactions on Automatic Control, vol.53, No.2, pp. 586-591, 2008.

[12] Cao, C. and N. Hovakimyan, "Guaranteed Transient Performance with L_1 Adaptive Controller for Systems with Unknown Time-varying Parameters and Bounded Disturbances." American Control Conference, pp. 3925-3930, 2007.

[13] Cao, C. and N. Hovakimyan, Stability Margins of L_1 Adaptive Control Architecture , IEEE Transactions on Automatic Control, vol.55, No.2, pp. 480-487, 2010.

[14] Hovakimyan, N. and C. Cao. *L_1 Adaptive Control Theory*, Society for Industrial and Applied Mathematics, Philadelphia, PA, 2010.

[15] Kaminer, I., Pascoal, A., Xargay, E., Cao, C., Hovakimyan, N., and Dobrokhodov, V., "3D Path Following for Small UAVs using Commercial Autopilots augmented by L_1 Adaptive Control," Submitted to Journal of Guidance, Control and Dynamics.

[16] Wise, K., E. Lavretsky, N. Hovakimyan, C. Cao, and J. Wang., "Verifiable Adaptive Flight Control: UCAV and Aerial Refueling," AIAA 2008-6658, AIAA Guidance, Navigation, and Control Conference, Honolulu, HI, 2008.

[17] Wang, J., C. Cao, N. Hovakimyan, R. Hindman and D.R. Ridgely, "L_1 Adaptive Controller for a Missile Longitudinal Autopilot Design," AIAA 2008-6282, AIAA Guidance, Navigation, and Control Conference, Honolulu, HI, 2008.

[18] Kharisov, E., I.M. Gregory, C. Cao and N. Hovakimyan, "L_1 Adaptive Control Law for Flexible Space launch Vehicle and Proposed Plan for Flight Test Validation," AIAA 2008-7128, AIAA Guidance, Navigation, and Control Conference, Honolulu, HI, 2008.

[19] Shah, G. "Aerodynamic Effects and Modeling of Damage to Transport Aircraft." AIAA-2008-6203 AIAA Guidance, Navigation, and Control Conference, Honolulu, HI, 2008.

[20] Wise, K.A., Lavretsky, E., Zimmerman, J., Francis, J.H., Dixon, D., and Whitehead, B., "Adaptive Flight Control of a Sensor Guided Munition" AIAA-2005-6385. AIAA Guidance, Navigation, and Control Conference, San Francisco, CA, August 2005.

[21] Sharma, M., E. Lavretsky, and K.A. Wise, "Application and Flight Testing of an Adaptive Autopilot on Precision Guided Munitions," AIAA-2006-6568, AIAA Guidance, Navigation, and Control Conference, Keystone, CO, August 2006.

[22] Reconfigurable Systems for Tailless Fighter Aircraft – RESTORE, Final Report, AFRL-VA-WP-TR-99-3067.

[23] Wise, K., and J. Brinker, "Reconfigurable Flight Control for a Tailless Advanced Fighter Aircraft," AIAA Guidance, Navigation and Control Conference, Boston, MA, August, 1998.

[24] Wise, K., J. Brinker, A. Calise, D. Enns, M. Elgresma, and P. Voulgaros, "Direct Adaptive Reconfigurable Control for a Tailless Advanced Aircraft," Int. Journal of Robust Nonlinear Control, vol. 9, pp. 999-1012, 1999.

[25] Brinker, J. and K. Wise, "Flight Testing of a Reconfigurable Flight Control Law on the X-36 Tailless Fighter Aircraft," AIAA Guidance, Navigation and Control Conference, Denver, CO, August 2000.

[26] Leman, T, E. Xargay. G. Dullerud, N. Hovakimyan, T. Wendel, "L_1 Adaptive Control Augmentation System for the X-48B Aircraft," AIAA Guidance, Navigation and Control Conference, Chicago, Il, August 2009.

[27] Griffin, B. J., J. J. Burken, E. Xargay, "L_1 Adaptive Control Augmentation System with Application to the X--29 Lateral/Directional Dynamics: A MIMO Approach", AIAA Guidance, Navigation, and Control, Toronto, Canada, 2010.

[28] Gregory, I. M., C. Cao, E. Xargay, N. Hovakimyan and X. Zou, "L_1 Adaptive Control Design for NASA AirSTAR Flight Test Vehicle," AIAA Guidance, Navigation and Control Conference, Chicago, IL, August 2009, AIAA-2009-5738

[29] MIL-STD-1797A, Anonymous, "Military Standard, Flying Qualities of Piloted Vehicles," 1990.

[30] Cunningham, K. "AirSTAR Flight Test Plan: 5.5 % Dynamically Scaled GTM Tail Number T2. Deployment: 2010.02." GTMP-6326 2010.02, V 2.00, May 24, 2010.

[31] Cunningham, K. "AirSTAR Flight Test Cards, v2.10." GTMP-6325 2010.02, V 2.10, May 27, 2010.

[32] Li, D., N. Hovakimyan and C. Cao, "Positive Invariance Set of L_1 Adaptive Controller in the Presence of Input Saturation", AIAA Guidance, Navigation, and Control Conference, Toronto, Canada, 2010.